OPERANDO ANALYSIS OF LITHIUM PLATING IN LITHIUM-ION CELLS

by

Tanay Adhikary

A Thesis

Submitted to the Faculty of Purdue University

In Partial Fulfillment of the Requirements for the degree of

Master of Science in Mechanical Engineering

School of Mechanical Engineering

West Lafayette, Indiana

December 2019

THE PURDUE UNIVERSITY GRADUATE SCHOOL
STATEMENT OF COMMITTEE APPROVAL

Dr. Partha P. Mukherjee, Chair
School of Mechanical Engineering

Dr. Amy Marconnet
School of Mechanical Engineering

Dr. Jason Ostanek
School of Engineering Technology

Approved by:
Dr. Nicole Key

To my Family

ACKNOWLEDGMENTS

To excel and develop in a field one must have a sense of security and authority with the essence of responsibility. There are always people associated who help and guide for the successful achievement of the desired objective. I would like to express my sincerest gratitude to my committee chair, Dr. Partha P. Mukherjee for having faith in me and guiding me throughout my coursework and research. I would also like to thank my advisory committee members, Dr. Amy Marconnet and Dr. Jason Ostanek for their valuable inputs and willingness to serve in this capacity.

A word of encouragement during a failure is worth more than an hour of praise after success. Special thanks to my lab mate and peer mentor Conner Fear for being the source of encouragement when things went downhill. His extreme inspiration and generous affection have brought this project to completion. I would also like to extend my appreciation to Daniel Juarez Robles, Mukul Paramananda, Ankit Verma, Anjul Arun Vyas, Sobana Rangarajan for their valuable inputs.

I would also like to take a moment and appreciate the remarkable infrastructure and resources of Purdue University, West Lafayette that provided me with access to the highly equipped laboratories and all the valuable books and journals without which this thesis would have been impossible to complete.

TABLE OF CONTENTS

LIST OF TABLES

LIST OF FIGURES

ABSTRACT

The widespread commercialization of electric vehicles is currently hindered by their inability to compete with conventional gasoline-powered vehicles in terms of refueling time. The main barrier to achieving fast charge of lithium-ion batteries is the plating of metallic lithium on the surface of the graphite negative electrode, which is known to occur most prevalently at high C-rates, low temperatures, and high states of charge (SOC). While it is accepted that the lithium plating process is largely reversible, the factors affecting the reversibility of lithium plating have not been thoroughly investigated. This work seeks to determine the most influential factors affecting the reversibility of lithium plating in order to devise strategies to mitigate long-term damage to the cell if lithium plating has been detected. It was determined that the temperature during the rest phase following plating has the most significant influence on plating reversibility, with cells undergoing rest at 30 ℃ exhibiting nearly twice the Coulombic inefficiency of cells undergoing rest at 0 ℃. Additionally, a novel technique was developed to observe the relaxation processes directly in a graphite electrode just after lithium plating has occurred. The occurrence of electrochemical stripping and the dissolution of overshooting phases in graphite were verified through direct *in-situ* observation. A two-part model is presented to describe the progression of the relaxation processes in graphite after lithium plating occurs under high rate operation.

CHAPTER 1 – INTRODUCTION

1.1 Why do we need Energy Storage Systems?

Ever since the industrial revolution, mankind has made tremendous advancement in terms of science and technology which has significantly improved the quality of human life. With every patent and scientific paper, we have progressed into a more convenient world with a better understanding of physics that governs our world. However, this technological advancement has led to the ever-increasing demand for energy. Our society has relied heavily on non-renewable forms of energy such as coal, natural gas, and petroleum to satiate the energy demand. This continued reliance on fossil fuels leads to the rapid depletion of the vast reserves of fossil fuels and the contamination of the environment through pollution.

Shifting to sustainable forms of energy is the most pressing challenge of our world now that is required to be solved. A cleaner alternative option to satiate this energy requirement is the usage of renewable forms of energy. Solar Energy, Wind Energy, Hydroelectric Energy, Geothermal Energy, Biomass Energy are some of the renewable forms of energy mankind is trying to shift to. Even though these provide the cleanest forms of energy, fluctuations in their availability make it difficult to continually harness them. Rising in tandem with the proliferation of technologies harnessing renewable energy are advanced energy storage systems. Energy storage systems provide the best way to circumvent this problem and provide a continuous supply of energy during off-peak hours or in locations ill-suited for harvesting a renewable form of energy. As the research in energy storage systems flourishes, the reliance on renewable forms of energy would become much more feasible.

1.2 History of Lithium-Ion batteries

In 1800 the first battery namely the “Voltaic cell” was made by an Italian scientist named Alessandro Volta. After that William Cruickshank came up with the first electric battery capable of mass production[1]. Ever since that the application of batteries flourished and it was commercialized rapidly. An important upgrade in the battery research was made by the invention

of the Daniell cell by the British scientist John F. Daniell. The Daniell cell had an operating voltage of 1.1V and a better life than the Voltaic cell. All these cells were primary cells. Primary cells can be only used once and can't be cycled after it has been exhausted. The electrochemical reaction in primary cells is irreversible. These cells are still used primarily for one-time use applications. MnO_2 is one of the primary cells were widely used.

Gaston Plante first discovered the first rechargeable battery which was based on a lead and acid system which still finds use today. The electrochemical reactions taking place in a rechargeable cell are reversible. These cells are also known as secondary cells. In terms of secondary cells, the Lead-acid secondary cell and the Nickel-based secondary cell were the ones primarily used although there were a large number of battery systems invented in the last century. The research on the advancement of battery systems rapidly proliferated. The invention of the lithium-ion battery was in response to the increasing demand for high-performance batteries. Lithium-ion batteries have high energy density and excellent cycle life. The lithium-ion battery system started catching up with high-end applications and gradually ended up becoming the state of art commercialized battery system.

1.3 Lithium-Ion batteries- the front-runner of Energy Storage Systems

Since the 1990s, Lithium-Ion batteries began replacing NiMH batteries and gradually became the front-runners of secondary battery systems. Lithium-ion batteries have a ubiquitous influence when it comes to energy storage applications. They are widely used in a variety of energy storage applications such as electric vehicles (EV), hybrid electric vehicles (HEV), Plug-in Hybrid electric vehicles (PHEV), portable electronics and green grid energy storage. Lithium-ion batteries have been flourishing in the battery market because of its high power and energy density, no memory effect and excellent cycle life. Thus, the demand for Lithium-Ion batteries has been growing at an unprecedented rate. Portable power supplies have become the lifeline of the modern technological world.

The electrical energy stored by a battery is usually expressed in terms of Energy Density per unit weight. This is a function of the cell potential (V). The maximum energy that could be obtained from a battery is primarily influenced by the type and the amount of active materials used.

However, depending on the kind of material used, there is a maximum theoretical capacity possible in absolutely ideal conditions. However, in real life, only a fraction of the theoretical capacity of the battery is achieved.

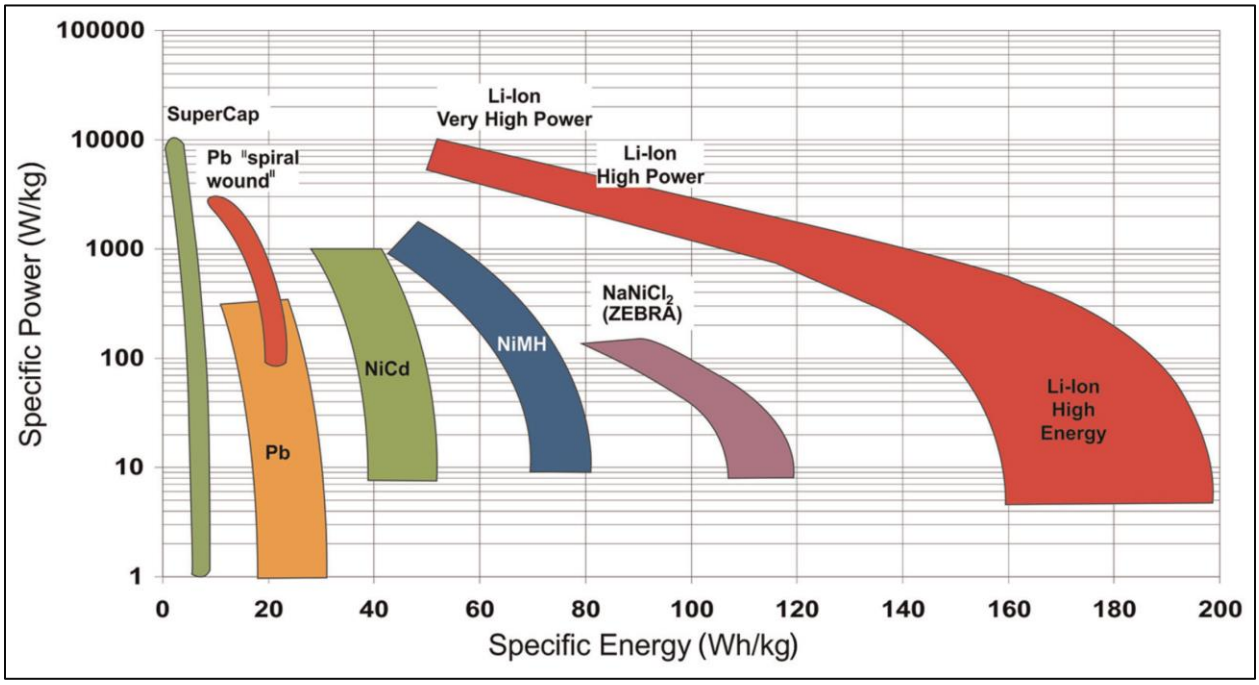

Fig 1.1: Ragone plot of various battery technologies [2]

Not only is lithium smaller in size, but it is also lighter in weight with a high theoretical energy density which is why it is regarded as the front runner of all the other battery systems. Fig 1.1 illustrates that lithium-ion battery technology has attained the highest gravimetric energy and power density among all the commercialized rechargeable battery technologies. Lithium-ion batteries offer high Coulombic efficiency values even at high current rates[2].

1.4 Types of commercially available Lithium-ion cells

Lithium-Ion batteries are available in formats. The key components can be packaged in different ways. There are three main categories in which lithium-ion batteries can be classified in terms of packaging:

1. Cylindrical Cells
2. Pouch Cells
3. Coin Cells
4. Prismatic Cells

1.4.1 Cylindrical Cell

The cylindrical cell is one of the most widely used packaging styles that has been implemented in lithium-ion batteries. Fig 1.2 shows the cross-section of a cylindrical lithium-ion cell.

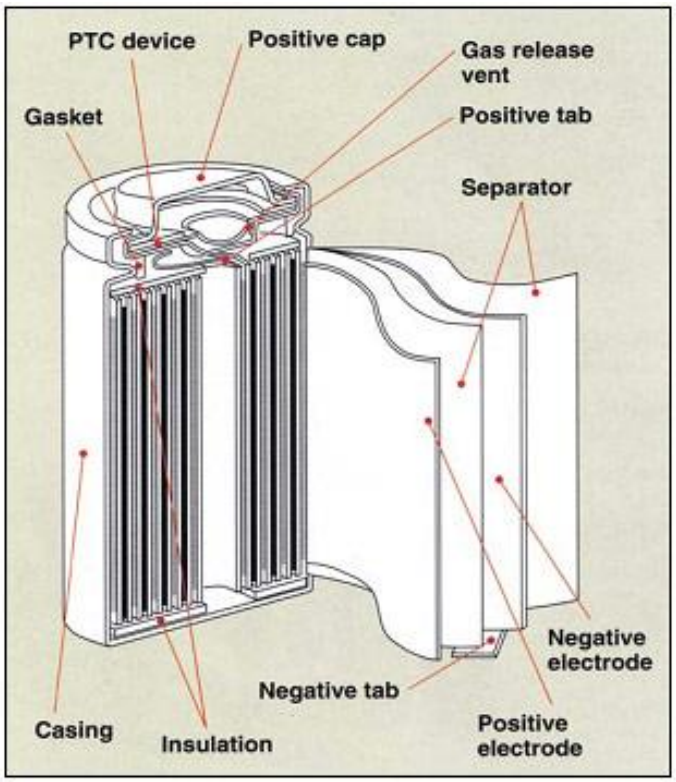

Fig 1.2: Schematic of the structure and components of a Cylindrical Cell[1]

The electrodes are cut into a long strip with dimensions in accordance with the dimensions of the battery. The electrodes are arranged in by placing the separator in between the anode and the cathode and this whole arrangement is placed between two sheets of spacers. This whole unit is rolled and fitted into a cylindrical casing. This type of cell provides excellent mechanical stability and is its fabrication is relatively simple. There are various dimensions of cylindrical cells which are as follows:

Table 1: Types of Cylindrical cells

Size	Dimensions
A cell	17 x 50 mm
AA cell	14.5 x 50 mm
AAA cell	10.5 x 44.5 mm
AAAA cell	8.3 x 42.5 mm
18650	18 x 65 mm
26650	26 x 65 mm
26700	26 x 70 mm
21700	21 x 70 mm

Another fascinating feature about cylindrical cells is the inclusion of a venting mechanism as shown in Fig 1.2. This mechanism is utilized when excess pressure is developed inside the battery due to the evolution of gases. This mechanism vents out the excess gases when the pressure crosses a particular threshold value based on its design.

1.4.2 Pouch Cell

A pouch cell is made up of multiple cell units comprised of anode and cathode with a separator in between, stacked upon one another with conductive tabs welded to the anode and cathode current collectors. A pouch cell is known to have the highest packing efficiency of around 95%. Fig 1.3 shows the schematic of the structure and components of a pouch cell[4]

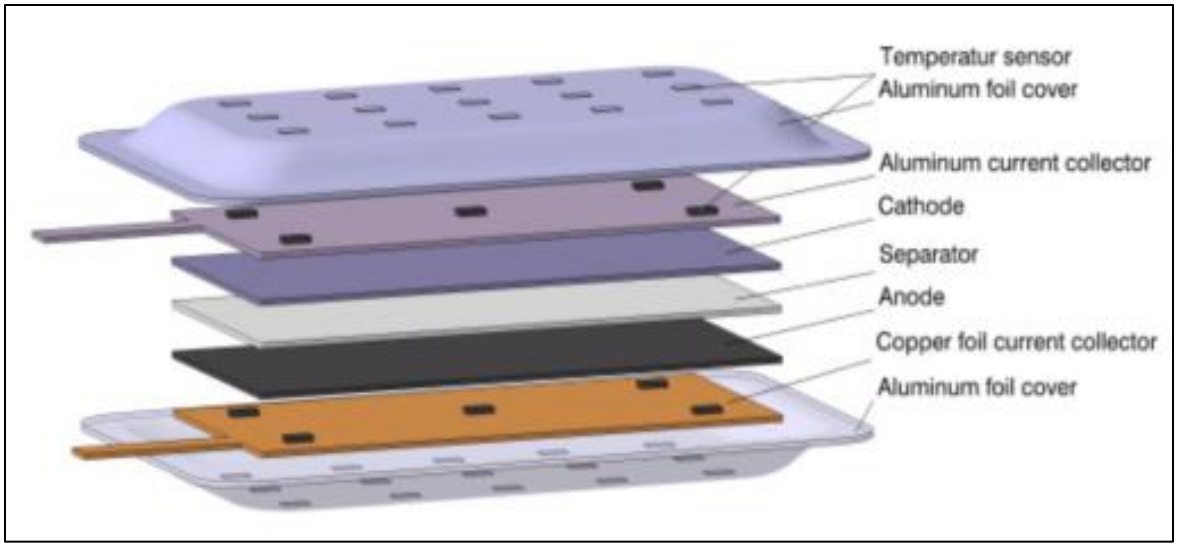

Fig 1.3: Schematic of the structure and components of a Pouch Cell[1]

The mechanical stability of a pouch cell is less in comparison to cylindrical cells due to the absence of the individual cylindrical casing. This makes the pouch cell lighter in weight. However, generally, a casing or mechanical support is provided in the fitting.

A serious concern regarding pouch cells is swelling due to the evolution of gases within the cell. The swelling of cells can result in adding mechanical stress to the device. This often results in damaging the equipment that is being powered by the battery. For example, if it is used in any electronic device, it might end up causing cracks or breakage to adjacent components like the LCD.

1.4.3 Coin Cell

Another commonly used format of lithium-ion battery is the coin cell which is also commonly known as a button cell. Coin cells come with a more compact design and are primarily used for smaller devices. To achieve the desired voltage, usually coin cells are stacked above one another.

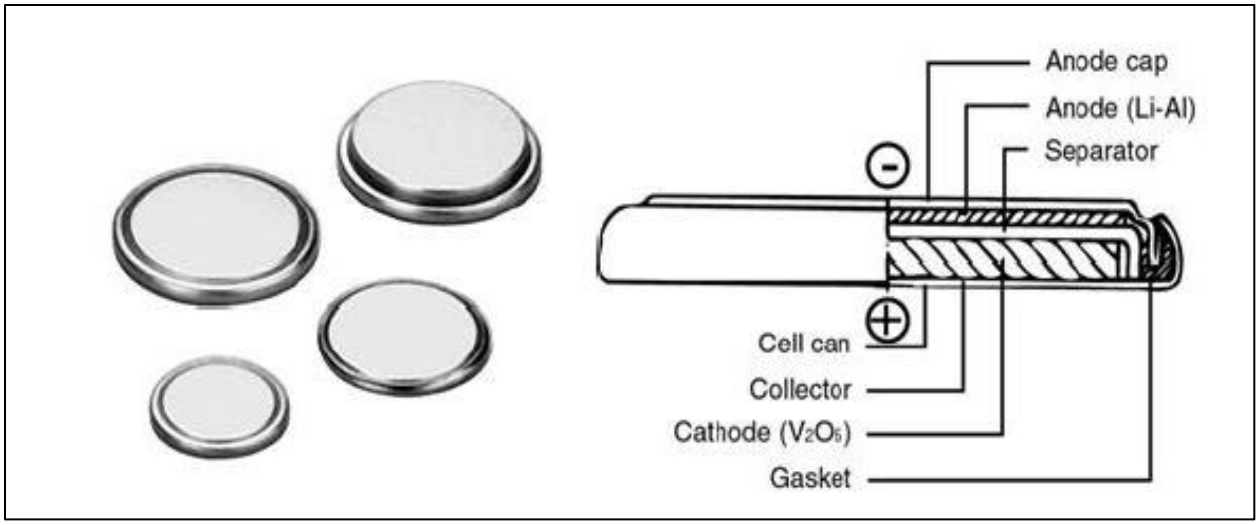

Fig 1.4: Schematic of the structure and components of a Coin Cell [1]

Fig 1.4 shows a coin cell and the various components that it is comprised of. Coin cells are usually inexpensive and come with a long shell life. They find applications in devices like calculators, watches and medical equipment.

1.4.4 Prismatic Cells

Prismatic Cells are predominantly found in mobile phones. The design of these cells is flexible and could be adjusted to accommodate the design of the product which the battery would be powering. Fig 1.5 shows the structure of a typical prismatic cell and the components it is comprised of.

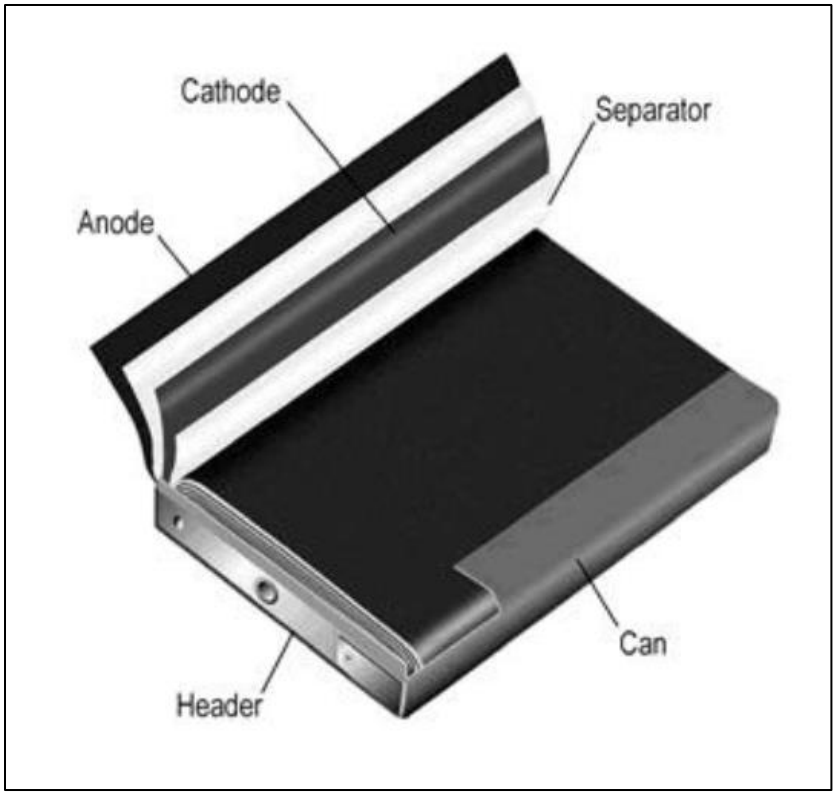

Fig 1.5: Schematic of the structure and components of a Prismatic Cell[1]

The modern prismatic cells are packaged in a soldered aluminum housing which is manufactured slightly thicker to account for the compromised mechanical stability in comparison to the cylindrical design. Prismatic cells usually offer relatively poor thermal management and usually has a shorter life cycle than its cylindrical counterpart.

1.5 Lithium-Ion battery electrochemistry

Even in the different type of commercialized Lithium-ion batteries, there are four functional components that are found in every type of Lithium-ion cells:

1) Anode
2) Cathode
3) Electrolyte
4) Separator

1.5.1 Anode

The anode is the negative electrode of an electrochemical cell. In order to strive for high energy density batteries, it is crucial to deploy high capacity electrode materials.

Initially, for secondary batteries, lithium metal was used as an anode. Alkali metals like Lithium could be a good prospect for negative electrodes. Higher voltage ranges can be obtained if lithium metal is used as an anode material since it has the lowest possible potential of 0.0V vs Li/Li^+. Lithium has a high specific capacity of 3862mAh/g due to its low density. However, there were various safety issues concerning the usage of lithium metal as anode material. During the charging process, several dendrites are formed which might pierce through the separator and cause internal shorting which consequentially might lead to the catastrophic event of a thermal runaway. Apart from that, Lithium metal reacts with the electrolyte and upon repeated cycling, it leads to the severe degradation of the lithium electrode.

With progressive research, the state-of-the-art anode material kept changing as researchers strived to obtain materials with higher capacity and fewer safety concerns. It was found that carbonaceous materials served as a better alternative for anode material. The first carbonaceous anode material used for battery commercialization was Coke. Later on, Coke was replaced with MCMB (MesoCarbon MicroBeads) since they provided a higher capacity per unit weight. However, S. Hossain et al. [5] explored the properties of C-C (Carbon-Carbon) composite and endorsed it as a strong candidate for the anode in lithium-ion batteries.

The ideal carbonaceous material is expected to have a high capacity, high electronic conductivity, and excellent lithium hosting capability. The application of novel technologies has been successful in improving the electrochemical performance of carbonaceous materials. E. Endo et al. [6] reported that the application of electron beam irradiation can improve the electrochemical performance of carbon electrodes by increasing the reversible capacity and also reducing the amount of structural changes during cycling.

At present, the most widely used anode material is Graphite. In comparison to Lithium metal, Graphite relatively has significantly lower capacity. Buqa et al. [7] explored the surface modification of graphite by the use of gas treatment at high temperatures and silylation in a nonaqueous solution that resulted in the reduction in the irreversible capacity loss. Natarajan et al [8] found that mild milling could be a good way to improve the reversible capacity and the faradaic

efficiency during the first formation cycle of graphite. Silicon is another material that was considered as an alternative for graphite. Silicon has a high theoretical capacity of 4200 mAh/g. However, the primary concern with Silicon is its high expansion and contraction during a typical charge-discharge cycle which makes its implementation difficult.

The state-of-the-art anode material used in a lithium-ion battery is graphitic carbon. The graphite is mixed with a conductive additive and a binder material and coated on a thin copper foil current collector. Graphite is an intercalation compound where the lithium diffuses into the graphite without a significant expansion in the overall volume. The electrochemical properties that make graphite a superior anode material will be discussed in a later chapter.

1.5.2 Cathode

The cathode is the positive electrode of an electrochemical system. The cathode electrode material like the anode plays a vital role in terms of determining the state of health of the battery. The cathode undergoes intensive structural changes during a typical charge-discharge cycle. The ideal cathode material should possess high electronic conductivity, high lithium ion diffusivity, high free energy of reaction with lithium and the ability to incorporate large quantities of Lithium. It should also have a lower chemical potential with respect to Lithium so that the cell's maximum voltage could be maximized.

The typical material used for the cathode is a metal oxide. The most common cathode material used is $LiCoO_2$ which is commonly known as LCO. LCO forms a layered structure that facilitates the swift diffusion of Lithium ions from the cathode during the charge-discharge cycle. Although it is successfully implemented in commercially available cells, Cobalt is expensive, and its availability isn't abundant. LCO also has a violent thermal runaway. Hence, there are ongoing research works to find alternatives and improve stability.

Another popular cathode material that was heavily researched is $LiMn_2O_4$. This material has a spinel structure. In this type of structural arrangement, the Lithium fills up the tetrahedral sites while the Manganese fills up the octahedral sites[3]. $LiMn_2O_4$ is relatively cheaper and safer to use than LCO. Although the major challenge towards the implementation of this material is its nature of undergoing phase change during cycling.

Another promising cathode material is $LiFePO_4$ with an olivine structure. In this type of structure phosphorus fills up the tetrahedral sites, Iron occupies the octahedral sites and lithium forms one-dimensional chains.[9] $LiFePO_4$ is a favorable choice because it is relatively inexpensive and Iron is less toxic in comparison to the other materials used as cathodes. $LiFePO_4$ has a theoretical capacity of around 160 mAh/g and it operates around the voltage of 3.5V. $LiFePO_4$ has a low energy density, however, it is less susceptible to thermal variations and provides a higher level of safety in comparison to LCO cathodes.

1.5.3 Electrolyte

The electrolyte is responsible for shuttling the Lithium ions from cathode to anode and vice versa during a charge-discharge cycle. The electrolyte is an intrinsic component of the cell and it heavily influences the cycle life of the cell. Ideally, it should have a high ionic conductivity to minimize the resistance in the transport of lithium ions during cycling. Another important characteristic that an electrolyte is that it should be electrochemically inert towards the electrodes during the operational voltage window.

An electrolyte typically consists of a mixture of liquid solvents and lithium salts. Common salts that are used are $LiPF_6$, $LiB(C_2O_4)_2$ and $LiBF_6$. The most commonly used salt is $LiPF_6$. Usually, the liquid solvents used are non-aqueous. Organic solvents such as Ethylene carbonate (EC) and Dimethyl Carbonate (DEC) are used. A mixture of the aforementioned solvents results in lower viscosity and higher ionic conductivity[10]. The presence of Ethyl Carbonate is crucial for the formation of a favorable SEI layer on the graphite anode.

1.5.4 Separator

The separator is one of the most crucial components of the cell that ensures the safety of the cell. It is a thin porous membrane that prevents the direct physical contact of the anode and the cathode. The separator is an ionic conductor which means it allows the lithium ions to pass through itself during to electrode it is intended to be traveling to depending upon the operation. It should be an electronic insulator and it should be chemically stable with respect to the electrolyte and the electrode materials.

Polypropylene (PP) and Polyethylene (PE) are some of the commonly used separators for commercial cells. Usually, these separators do not lose their properties even after repeated cycling. Sometimes both the materials are used in the fabrication of a separator. This is usually done to facilitate separator shutdown during anomalous circumstances that are expected to lead to a thermal runaway. The presence of Polypropylene and Polyethylene offers different melting points. At the event of the heating up of the cell, one of the layers of the separator melts first due to the difference of the melting point of the two layers. At this point, the cell experiences a shutdown since the separator starts behaving as an insulator. Consequentially it reaches a shutdown point thereby preventing the thermal runaway of the cell.

1.6 Working of Lithium-Ion batteries

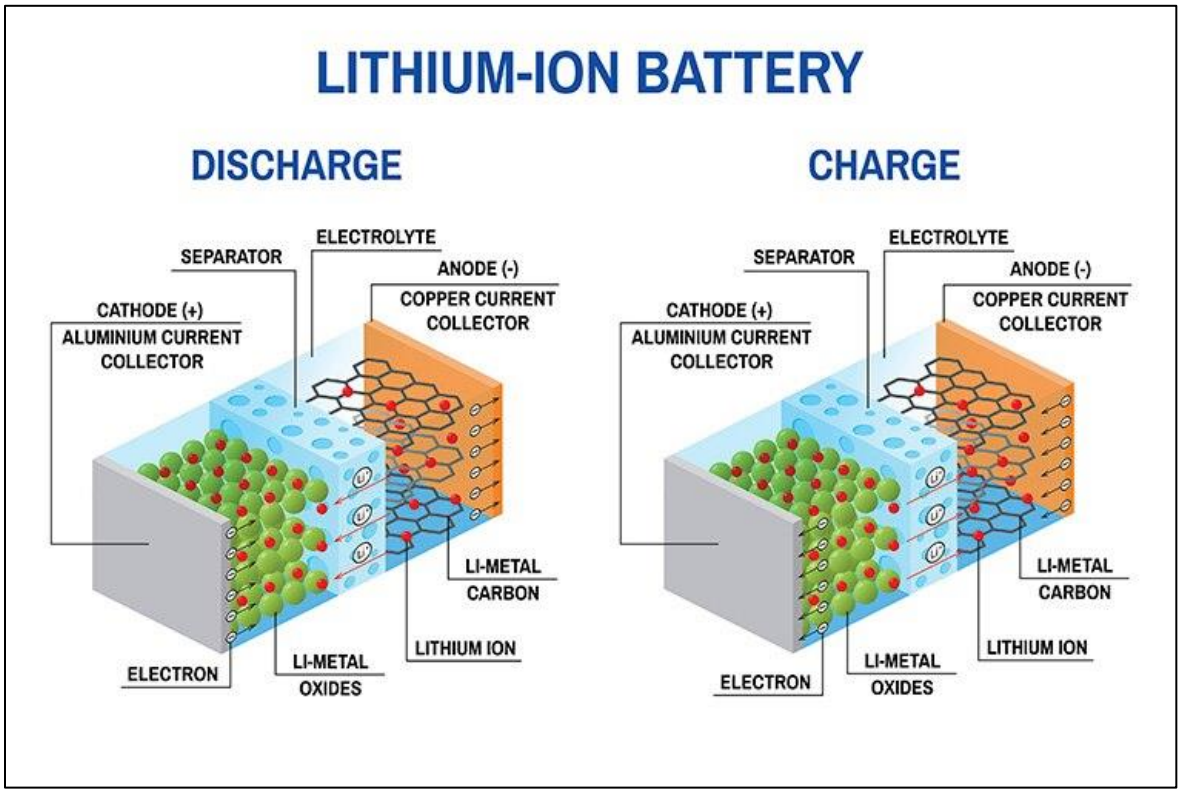

Fig 1.6: Schematic of the working of a lithium-ion battery during charging and discharging [11]

The lithium-ion battery is an advanced battery technology that is finding a wide variety of uses in different applications. As the name suggests, lithium ions are used as the key component of the electrochemistry. In a lithium-ion battery, the Li^+ ions shuttle between the two electrodes while in order to balance this an equivalent number of electrons flow through the external circuit.

In reference to Fig 1.6 during charging, the electrical energy supplied is converted into chemical energy stored in the cell. An external current or potential is applied to the circuit as shown. Li atoms at the cathode are electrochemically oxidized and the positively charged Li+ ions that are extracted from the cathode flow through the separator in the electrolytic medium to the anode. The electrons move in the external circuit from the cathode current collector to the anode current collector to maintain the balance of the charge. For Li-ion batteries, the anode material is generally an intercalation compound (usually graphite). The Li^+ ions, upon reaching the anode, are reduced and intercalate into the anode material. When the anode material reaches its intercalation limit it can be said that the lithium-ion battery is fully charged. During the charging cycle, oxidation takes place at anode and reduction takes place at the cathode. The redox reactions for a typical Li-ion cell has been included below:

Negative Electrode: $C_6 + xLi^+ + xe^- \leftrightharpoons Li_xC_6 \ (0 \leq x \leq 1)$ Equation 1.1

Positive Electrode: $LiMO_2 \leftrightharpoons Li_{1-x}MO_2 + x\,Li^+ + xe^-$ Equation 1.2

During discharging, the chemical energy stored in the cell is converted into Electrical Energy. A potential difference is applied across the terminals of the battery that draws current from the battery. The lithium that is intercalated in the anode material is oxidized into Li+ ions. These Li+ ions now flow past the separator towards the cathode to be reduced back to Li. To balance this, electrons flow through the external circuit. This electron flow through the external circuit is the usable current that could be used to power the device that the battery is intended to provide power to.

1.7 Degradation Mechanisms in Lithium Ion Batteries

The major degradation mechanism in Lithium-Ion batteries are:

(i) Particle cracking

(ii) Loss of Li-ion inventory – a) SEI layer formation b) side reaction of lithium with electrolyte compounds.

(iii) Lithium Plating

Degradation mechanisms of Li-ion batteries are one of the most actively researched domains[12]. Li-ion batteries have been widely used in the automotive industry and the portable industry sector. The performance of the batteries used in these applications is influenced by the degradation mechanisms of lithium-ion batteries. The overall aging of the lithium-ion battery is influenced by the aging mechanisms of the individual battery components. For example, the binder and the electrolyte undergo decomposition, the separator undergoes melting, the current collector corrodes. Different modes of degradation are dominant in each electrode material due to its unique properties. Based on the commonly used materials at the cathode, the major degradation mechanisms are structural disordering due to loss of lithium inventory and metal dissolution. The most commonly used anode material in lithium-ion batteries is graphite. The major degradation mechanisms that the anode undergoes are degradation due to the loss of Lithium inventory, degradation due to the structural changes and lithium plating.

1. Lithium inventory loss- The loss of recyclable lithium ions upon repeated cycling could be because of two primary reasons.
    a. Formation of Solid Electrolyte Interphase layer: The Lithium and the electrolyte undergoes several unwanted side reactions to form compounds thus using consuming both the lithium inventory as well as the electrolyte. This results in low capacity retention and high Coulumbic Inefficiency. The consumption of the lithium inventory also reduces the ionic conductivity of the electrolyte as well as shifting the working potential of the cathode upward over repeated cycling. At some point, if the cathode is significantly de-lithiated the structure of the cathode can be irreversibly damaged. Furthermore, the cathode potential could exceed the

electrolyte stability window leading to the formation of a cathode electrolyte interface (CEI) layer which has the same deleterious effect as the SEI layer.

b. Dead Lithium: Dead Lithium is referred to as the lithium that is electrically isolated and no longer recyclable [13]–[15]. The occurrence of Dead lithium stems from the occurrence of dendrite formation whenever lithium is deposited in the form of metallic lithium. In lithium metal batteries where the anode material is lithium metal, we observe dendrite formation upon repeated cycling. The formation of dendrites increases the propensity of the detachment of lithium metal leading to electrical isolation [16]. This lithium is no longer usable implying the loss of recyclable lithium inventory.

2. Structural changes: Graphite has a hexagonal lattice structure. During the process of charging the Lithium ion intercalates into the lattice structure. When a lithium-ion battery is repeatedly cycled at a high C-rate, the repeated diffusion of the lithium ions into the graphite lattice structure induces mechanical strain. The insertion and re-insertion gradually disrupt the orientation of the graphite particles and can cause particle cracking, which exposes fresh surfaces of the graphite to the electrolyte and encourages further SEI formation.

3. Lithium plating- Lithium plating is the most dangerous and detrimental degradation mechanism that a lithium-ion battery undergoes during the charging cycles throughout its lifespan. In this process the incoming Li^+ ions deposits as metallic lithium on the surface of the Graphite instead of intercalating in the graphite. This occurs when there is a mismatch between the rate of the incoming Li^+ ions and the rate at which the Li^+ ions are diffused in between the layers of Graphite, most frequently occurring at low temperatures, high charge rates, and high states of charge (SOC).

Out of the degradation mechanisms discussed above, lithium plating is the major degradation mechanism that ends up in the failure of the cell especially due to the formation and growth of

dendrites. The formation and growth of dendrites may even lead to piercing the separator which is usually packed very tightly with the electrodes. Consequently, the cell is internally shorted that might trigger the thermal runaway ending in the catastrophic failure. Hence it is crucial to develop a strong fundamental understanding of lithium plating, its influencing factors, its nature and methods to mitigate the occurrence of Lithium plating.

1.8 Safety aspects of Lithium-Ion batteries

In recent years, lithium-ion batteries have been widely implemented but along with it came numerous safety-related incidents. It is these safety concerns that have impeded the wide scaled applications of lithium-ion batteries to its fullest potential. In 2008, the battery pack of a Toyota Prius which used lithium-ion batteries, caught fire due to thermal runaway while running on the highway [17]. In 2013, the battery pack of an auxiliary power unit of a Boeing 787 Dreamliner caught fire due to an internal short circuit [18]. One cell in the battery pack experienced thermal runaway due to internal short which further triggered thermal runaway in the adjacent cells. In 2016, Samsung Galaxy Note 7 was banned from carrying in flights since it caught fire [19]. It was speculated that the pouch cell deformed from the corners, resulting in the electrode tabs touching each other which led to the internal short-circuiting. This led to thermal runaway which resulted in the catastrophic event of fire/explosion.

Safety is a serious issue in lithium-ion batteries and it's a lesson we can learn from the various reports depicting the accidents regarding explosions and fires originating from thermal runaway. A thermal runaway is the most dangerous failure mode in a lithium-ion battery. The initiation of thermal runaway generally occurs due to elevated temperatures when the rate of a reaction goes out of control and as a chain effect the increased temperature further accelerates the reaction rate [20]–[22]. Lithium plating is one of the reasons that could trigger a thermal runaway. The growth of metallic dendrites is regarded as the primary safety concern that could trigger a thermal runaway[23]–[26]. However, M. Fleischhammer et al.[27] in their Differential Scanning Calorimetry (DSC) experiments not only observed a stronger exothermic reaction leading to a higher degree of destruction after the thermal runaway, but they also observed a low onset temperature (30-53°C) leading to thermal runaway under quasi-adiabatic conditions. In 2017, T.

Waldmann et al [28] carried out ARC tests and reported that in the event of lithium plating, the time until cell goes into thermal runaway is significantly reduced due to the occurrence of stronger exothermal reactions due to the presence of metallic lithium. Thus, it is evident that lithium plating is one of the primary precursors to thermal runaway which is the most severe catastrophic failure modes of a lithium-ion battery. In this thesis, this phenomenon of lithium plating has been extensively studied.

CHAPTER 2 – LITERATURE REVIEW: LITHIUM PLATING

2.1 Introduction

In a typical charging phase of a cell lithium ions deintercalated from the cathode and is transferred through the electrolyte to the anode material while the flow of electrons in the electrons in the external circuit balance this transfer. When the lithium ions reach the anode the path of least resistance for these lithium ions is intercalation into the graphite. Legrand et al. [29] report that the potential for intercalation of lithium into graphite lies in the range of 65 – 200 mV (vs Li/Li^+). Their work also says that when the anode potential drops below 0V (vs Li/Li^+) it becomes thermodynamically favorable for the lithium to deposit on the surface of the anode. Under ordinary conditions, the lithium plating reaction isn't a competitive reaction to the intercalation reaction [30]. However, the process of charging in real life is dynamic and not in equilibrium. The main reason behind this is the polarization of the anode which happens due to overpotentials like Ohmic drop, charge transfer overpotential, and diffusion overpotential. Arora et al. [31] observed that Li plating and lithium intercalation into graphite is a parallel reaction. The total charging current could be divided into the intercalation current and the plating current.

Intercalation reaction:

$$C_6 + xLi^+ + xe^- \rightarrow Li_xC_6 \ (0 \leq x \leq 1) \qquad \text{Equation 2.1}$$

Lithium plating reaction:

$$Li^- + e^- \rightarrow Li \qquad \text{Equation 2.2}$$

2.2 Graphite – An excellent Anode material

2.2.1 Reasons for using Graphite as the anode material

Graphite is the current state-of-the-art anode material that has been widely commercialized in various types of Lithium-ion batteries. Graphite has an excellent cycle life, convenient operating voltage window and relatively inexpensive. Graphite has a theoretical specific capacity of 372 mAh/g [32]. The performance of these graphite electrodes is heavily influenced by the way it is fabricated. Parameters like cycle life, capacity can significantly vary based on the additives like a binder and conductive additive used and also the electrode preparation technique employed. Such discrepancies in performance are observed since parameters like porosity, tortuosity and the overall electrical conductivity in the graphite network are influenced by the electrode preparation [33] [34].

Graphite is comprised of a giant covalent structure in which each carbon atom forms covalent bonds with three other carbon atoms. These carbon atoms form a hexagonal arrangement in a plane which forms one layer amongst the many other layers. The process of insertion of lithium ions within these layered structures due to the difference in the intraplanar and interplanar bonding forces is called intercalation[35]. Upon the intercalation of the lithium into the graphite, the graphite expands slightly in the direction perpendicular to the planes of the layers, without significantly increasing the volume of the anode.

A lot of research was reported in the literature in search of better anode materials. Several carbonaceous materials were investigated as suitors for anode materials. Carbonaceous materials when used as anode materials are less susceptible to dendrite growth associated with metallic lithium[36]. This increases the cycle life of the battery and improves the safety aspects of the battery as well. A promising carbonaceous anode material that was examined was Coke. However, in comparison to graphite, the lithium intercalating capability of cokes is less and neither do they form staged phases as observed in the case of graphite[37][38][39]. Ohzuku et al [35] studied several carbonaceous anode materials and found that graphite has a very low working voltage of 0 – 0.3 V Li/Li^+ and a very high volumetric capacity of 0.6 Ah cm^{-3}.

2.2.2 Stage Transition of Graphite

The intercalation process of lithium into graphite progresses by the sequential filling of the vacancies at periodic distances. As these vacancies get occupied the concentration slowly increases towards saturation.

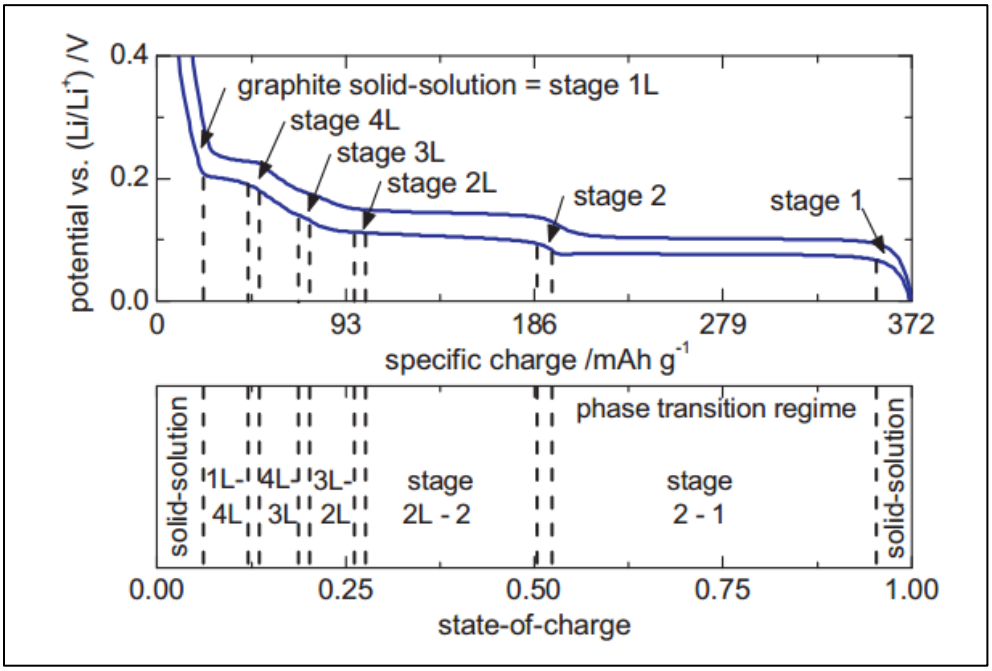

Fig 2.1: Stage transition in graphite during lithium intercalation [40]

Fig 2.1 shows the various phase transition that the lithium-graphite binary system undergoes during the process of charging of a cell. The stages are identified as we progress lithiating the graphite from a 0 – 100 SOC. Within the range of 0-25 % SOC, the existence of lithium is in a liquid-like phase. After Stage 2L is reached, the subsequent phase transition to Stage 2 occurs as the graphite becomes dense and ordered. As the lithiation progresses from Stage 2 to Stage 1 the lithium ions align in straight columns.

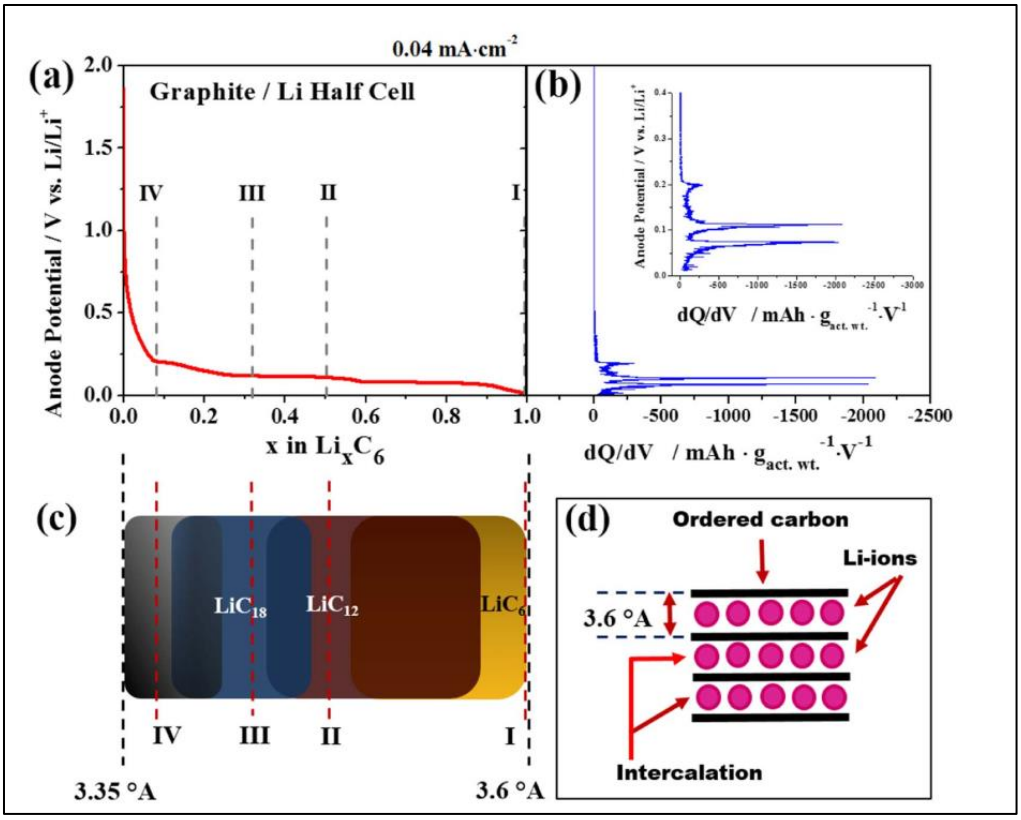

Fig 2.2: Color change observed as lithiation progresses [41]

As illustrated in Fig 2.2, the color of graphite changes as it transitions from one stage to the other upon lithiation [25]. The intercalation of lithium into the graphite is periodic and it forms different graphite intercalation compounds (GICs) at different degrees of lithiation which has their own characteristic color.

J. Wandt et al. [42] also reports about the color change when the cell is charged from 0 - 100% State of Charge for C-rates of C/10 and 1C as shown in Fig 2.3. The natural color of graphite (C_6) is black which is observed in the de-lithiated state. At the low rate of C/10, the entire electrode shows Stage 3 ($Li_{0.25}C_6$) which has the characteristic color of blue at 25% State of Charge. Thereafter, the entire electrode homogenously attains Stage 2 ($Li_{0.5}C_6$) having a characteristic color of red, before finally homogenously attaining Stage 1 ($Li_{1.0}C_6$) which has a golden color. However, the same homogeneity isn't observed for higher C-rates of 1C. Homogenous lithiation is observed at low states of charge. The lithiation is no longer spatially homogeneous due to the Ohmic drop at higher SOCs and that's the reason why multiple phases could exist spatially throughout the electrode.

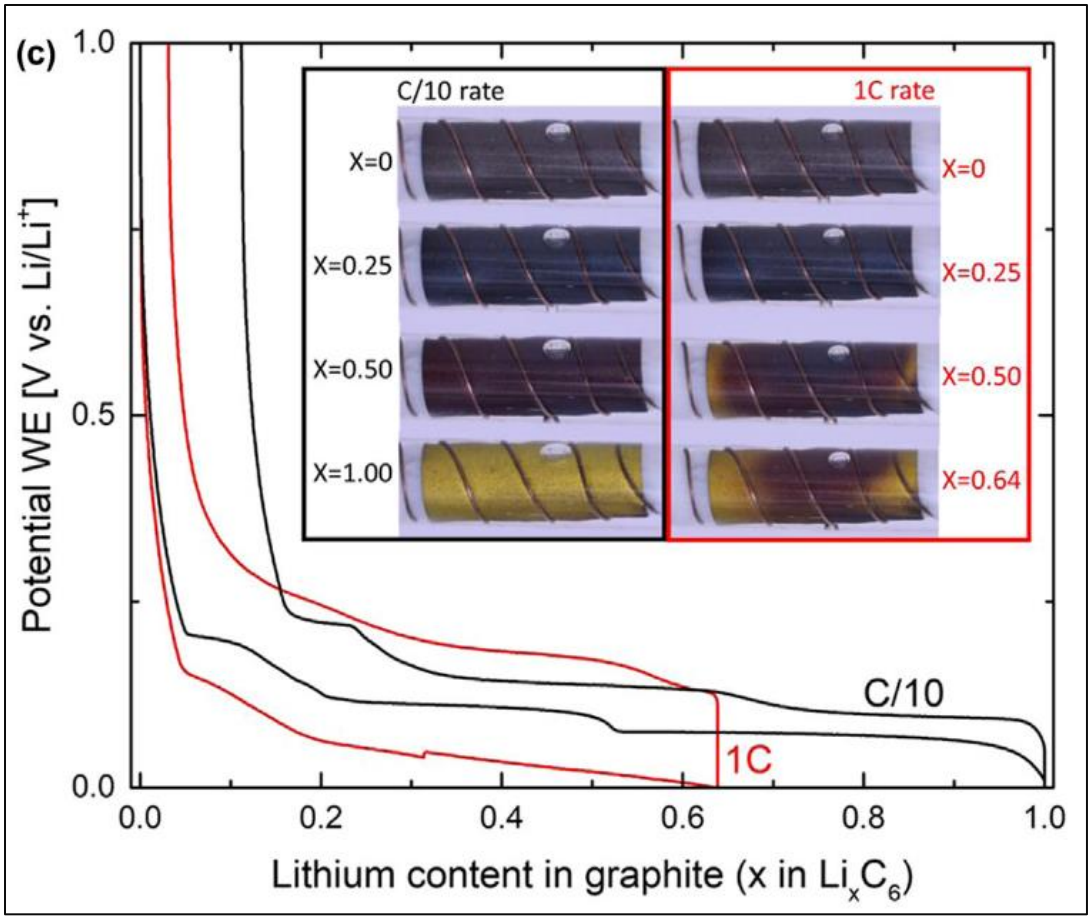

Fig 2.3: Operando EPR showing the color changes as Graphite is lithiated from 0-100% SOC at different C-rates (C/10 and 1C) with respect to the Anode potential vs Lithiation curve.[42]

Thus, color change of graphite upon lithium intercalation is a semi-quantitative measure for the SOC of Lithium as it could be understood from Fig 2.3. The color represents the concentration of the lithium that has been intercalated and it is not the measure of spatial dependence of the Li^+ concentration in the electrolyte[25].

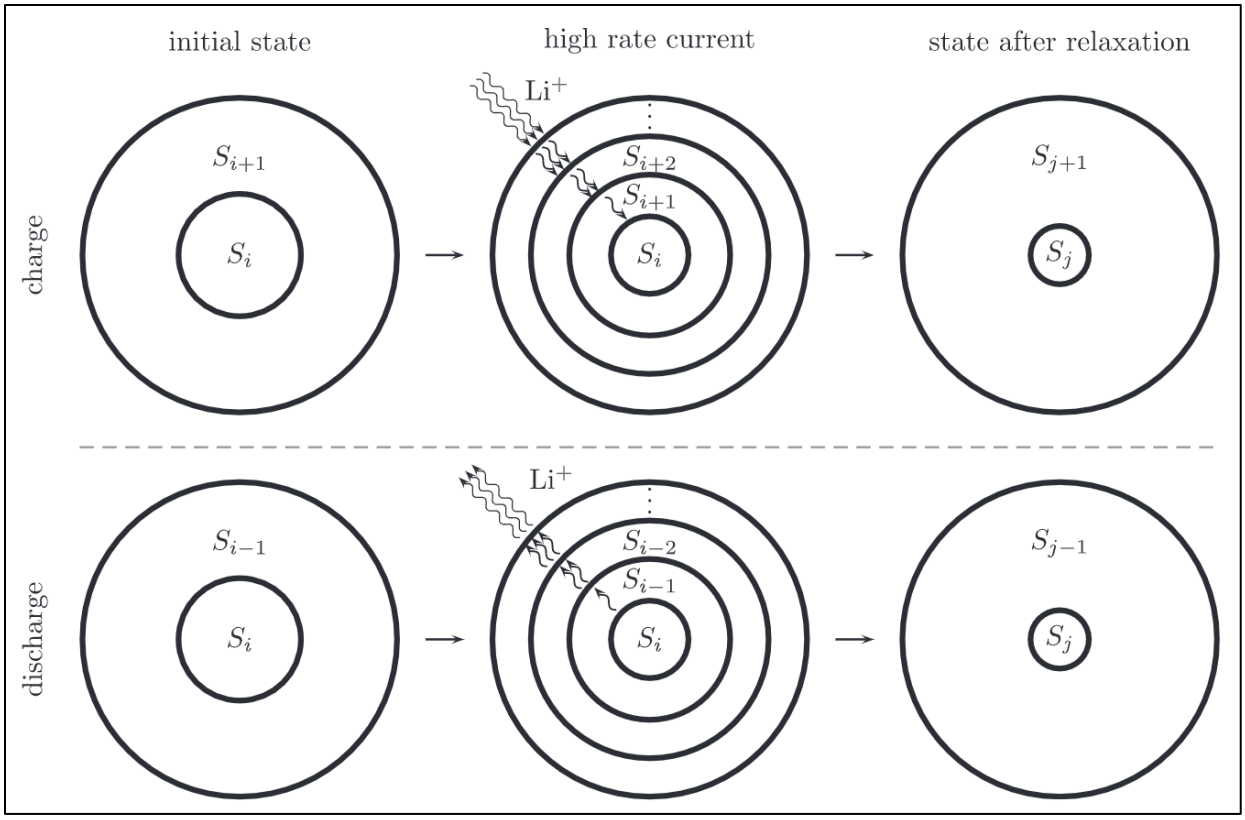

Fig 2.4: Schematic for the existence of multiple overshooting phases during lithiation of graphite at higher C-rates[43]

M. Bauer et al. [43][44] explains the existence of multiple overshooting phases during the lithiation of graphite at higher C-rates through a schematic as illustrated in Fig 2.4. Two phases of intercalation ($Stage_i$ and $Stage_{i+1}$) compounds are assumed to be coexisting at the beginning of a current pulse. During charging, graphite intercalation compounds with a higher degree of lithiation are preferentially located on the outside of the particle from where the lithium is coming in. At higher charging rates, the influx of lithium ion the external region of the particle is higher than the diffusion process inside the particle. This gives rise to the formation of a higher-order compound ($Stage_{i+2}$) even when the lithiation in the core of the particle is still lagging due to limited solid-state diffusion. In some cases, more than 3 stages are observed since, under non-equilibrium conditions, Gibbs' two-phase rule is not valid.

2.2.3 Solid Electrolyte Interface (SEI) layer formation

An important characteristic of using graphite as an anode material is the fact that the lithium-graphite intercalation compound forms a Solid Electrolyte Interphase (SEI) layer which was first named by Peled [45]. During the first charge-discharge cycle which is known as the formation cycle, a part of the lithium that intercalates into the graphite will react with the organic electrolyte and form the SEI layer [46]. This is the reason why an initial irreversible capacity is observed during the first cycle. The SEI layer is an ionic conductor but an electronic insulator. The mechanism of the formation of the SEI layer was proposed by Besenhard et al. [47] which was bolstered by the works of Inaba [48], [49]. Nie et al. [50] investigated the structure and the composition of the SEI layer with an unique combination of multiple characterization techniques: TEM, NMR, XPS and FTIR spectroscopy and found out that the SEI layer is 50 nm thick which acts as a passivation layer preventing further electrolytic reduction. The composition, thickness of the SEI layer changes with cycling and ageing [51], [52].

2.3 Factors influencing Lithium Plating

The primary barrier to achieving fast charging in Li-ion batteries is the plating of lithium metal on the surface of the graphite anode. It occurs when the rate of lithium ion reduction at the graphite particle surface exceeds the rate of diffusion of lithium into the particle.

The propensity for the metallic lithium to deposit on the surface of the anode is influenced by the cell design as well as the operational parameters. Extensive research has been carried out to explore the effect of the parameters that influence Lithium plating. Some operational parameters that directly influence the tendency of lithium plating to occur are:

1). C-rate [33], [46], [49], [53]–[61]

2). Temperature [46], [53]–[57], [59], [60], [62]–[69]

3). State of Charge [13], [25], [46], [53], [59]–[61]

Waldmann et al [59] illustrate how these operational parameters influence lithium plating.

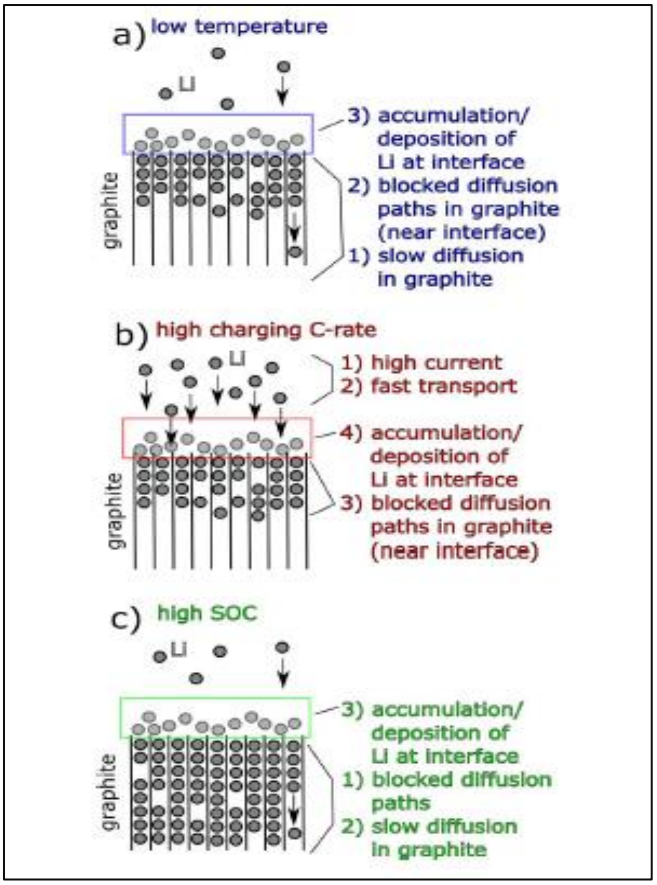

Fig 2.5: Schematic of the influence of the major operational parameters on lithium plating [59]

1) C-rate – The rate at which the battery is charged with respect to its maximum capacity, is defined by C-rate. A 1C rate means that the current will charge or discharge the entire cell in 1 hour. A C/2 rate means that the current will charge or discharge the entire cell in 2 hours. A 2C rate means that the current will charge or discharge the entire cell in 30 minutes.

Now with the increase in C-rate, the charging current would be increased, which means that the rate of incoming flux of Li+ ions will be higher. The rate of intercalation of these Li+ ions through the process of diffusion will fail to match up with the high incoming flux Li+ ions. Several researchers have reported that the solid-state diffusion of lithium into the graphite is limited at higher C-rates[65][66]. This increases the tendency of the deposition of metallic lithium on the surface of the anode.

2) Temperature - The chemical kinetics is a function of temperature which is governed by the Arrhenius equation. At low temperatures, the chemical kinetics slow down considerably which slows down the rate of diffusion of the lithium ions inside the Graphite anode thereby slowing down the rate of intercalation. When the rate of intercalation is slowed down it fails to match up with the rate of incoming Li+ ions. This increases the tendency of the deposition of the metallic lithium on the surface of the anode.

This is the reason why the implementation of lithium-ion batteries has struggled to flourish in cold-weather regions. Figuring out thermal strategies to overcome this problem has been widely researched. Some researchers have suggested the heating up the battery slightly before operation by a thermal system that is powered by an external source or by the battery itself[67], [70], [71].

3) State of Charge - The State of charge signifies the level of charge it is on relative to its capacity. With an increase in the state of charge, the number of available intercalation sites decreases. These intercalation sites are now filled with Lithium. This essentially blocks the diffusion pathways thereby increasing the tortuosity. The lithium diffusing in at a higher state of charge has much more difficulty in reaching its intercalation site and due to higher tortuosity, it has to take an indirect pathway which slows down the rate of diffusion. Thus, with the increase in the state of charge the rate of intercalation fails to match up with the rate of incoming Li+ ions. This increases the tendency of the deposition of lithium on the surface of the anode. As discussed earlier, graphite undergoes stage transition as lithium intercalates into it. Persson et al. [72] found from the first-principles calculations that the intraplanar Li diffusion in graphite becomes slowly difficult with the increase in Li concentration into the graphite.

Apart from these operational parameters, another factor that influences lithium plating is the defects associated with the design or the fabrication of the cell. L. Gireaud et al.[55] reported that the texture of the electrode surface influences the dendrite growth. A rough surface induces variation in the local current density on the electrode surface while a smoother texture would ensure a relatively homogenous distribution of current density. F. Hao et al. [73] report that in the

event of lithium plating, metallic lithium preferentially deposits over the surface protrusion at a higher rate thereby initiating Li dendrite formation.

The nature of electrolyte also plays a vital role in influencing lithium plating. Smart and Ratnakumar [68] reported that at low temperatures the diffusion of the lithium into the graphite is hindered if the electrolyte contains high Ethyl Carbonate formulations since it facilitates the formation of a pertinacious SEI layer that doesn't let the lithium pass through it easily.

In the event of an overcharge, despite the filling up of the interstitial vacancies in the graphite, there is an influx of lithium ions. At such events deposition of metallic lithium is observed at a SOC level greater than 100% [74]

2.4 Detection of Lithium Plating

Lithium plating is one major reason for safety concerns in lithium-ion which is has a significant impact in compromising the reliability and the longevity of the battery. Detection of lithium plating is a crucial step to assess the fundamentals behind the occurrence of this phenomenon. Mitigation catastrophic events can only be done when they could be detected beforehand. A substantial amount of research has been done in this aspect. The methods reported in the literature for the detection of lithium plating can be broadly classified into two major categories:

1. Destructive techniques
2. Non-destructive techniques

2.4.1 Destructive techniques

The methods to obtain direct evidence of metallic lithium deposition on the surface of the graphite anode usually involves in disassembling the cell. In 1996, D. Aurbach et al.[75] used X-ray Photoelectron Spectroscopy to study lithium deposition in lithium electrodes. Waldmann et al. [76] reviews the various post mortem analysis techniques that could be employed on lithium-ion cells after disassembly. It is advised to define the state of the cell at which it is opened as well as the disassembly environment to get the best result [76]. Hightower et al. [77] performs TEM analysis on the anode samples and employs a protection technique by covering the sample with Fluorinert

which is an inert liquid, before transferring it to the vacuum chamber. During charging, lithium plating and dendrite formation have been studied by in situ optical microscopy [24]–[26], [78]–[80]. Honbo et al. [81] studied lithium plating on graphite using Scanning Electron Microscopy and reported dendritic and granular morphologies of lithium deposition on the anode surface. Further, M. Zier et al. [82] reported that Osmium tetroxide staining could significantly improve the material contrast in the Electron Microscopy technique for the detection of lithium plating. Krämer et al. used Energy Dispersive X-ray spectroscopy mapping as the detection technique to analyze lithium plating. They modified the anode using isopropanol and detected for O and C in the formation of Li_2CO_3 which was further verified with Fourier-transform infrared spectroscopy and X-ray powder diffraction. In 2015, Ghanbari et al. [83] used Glow Discharge Optical Emission Spectroscopy depth profiling to detect metallic lithium deposition on the surface of the graphite electrode.

A lot of methods could be used as quantitative or semi-quantitative detection methods that provide us with information regarding the detection of lithium plating. However, in real-life applications, destructive methods are inconvenient and cannot be applied to battery management systems. Hence, it's crucial to look into non-destructive electrochemical techniques that could be used to detect and quantify lithium plating.

2.4.2 Non-destructive techniques

A lot of inference can be drawn from the analysis of electrochemical data obtained during the charging and discharging processes. One effective non-destructive method is the measurement of anode potential. Several researchers have reported the occurrence of lithium plating when the anode (graphite) potential drops below 0.0V (vs Li/Li^+)[57], [68], [78], [84]–[86]. The methodology commonly applied to monitor the anode potential is by the usage of a Li reference electrode in a three-electrode cell setup [87][88]. Alternate options for reference electrodes such as Li-Sn [89], Li-Al[90], $Li_4Ti_5O_4$ and $LiFePO_4$ [91]and in the three-electrode setup have been explored. The use of a reference electrode facilitates the monitoring of the potentials of the individual electrodes. Hence, the potential of the graphite electrode can be measured separately which gives us an insight into lithium plating. The use of a three-electrode cell would come with certain disadvantages. An ideal reference electrode should be such that it has a minimal influence on the regular operation of the cell. Y. Hoshi et al. [92] studied the optimum position to place a

reference electrode and concluded that the area which is outside the region between the anode and the cathode is optimum since it has a low potential gradient and low-frequency dependence of the potential. The localized current density distribution might be disturbed by the presence of a reference electrode even if it is electrochemically inert. It might result in the localized deposition of metallic lithium around that region.

Another in situ technique that is used to determine lithium plating is Electrochemical Impedance Spectroscopy [55].

In 2014, Bitzer et al [93] came up with a new method for detecting lithium plating by measuring the change in the cell thickness. Their study employed the usage of a measuring setup that had a resolution of 1μm. The volume change of the cell under regular operating conditions was measured for calibration to take into account the increase in thickness due to intercalation and gas evolution. In 2015, Birkenmaier et al. [94] performed a similar study using a laser triangulation setup for the detection of lithium plating by measuring the increase in the volume of the cell. In 2018, F.B. Spingler et al. [95] developed an in situ thickness measurement technique to detect lithium plating on the basis of volume expansion in pouch cells.

Another in situ technique which could be used to detect lithium plating is by monitoring the Coulombic Efficiency. Coulombic efficiency, which is also known as the Faradaic Efficiency, is defined as the ratio of the charge extracted from the battery to the charge put into the battery. During a typical charge-discharge cycle the capacity during the charging and discharging can be monitored. In the event of lithium plating, the consumption of lithium in reaction with the electrolyte or in the formation of dead lithium would show a drop in the Coulombic Efficiency. This principle is used in the detection of lithium plating using Coulombic Efficiency. In 2015, J.C. Burns et al. [96] uses high precision coulometry to detect the onset of lithium plating on both commercial 18650 cells and pouch cells.

Another technique that could be used for the detection of lithium plating is the analysis of electrochemical data during discharge and voltage relaxation. In the event of lithium plating, a high voltage plateau is observed during the subsequent discharging or rest phase. The occurrence of this high voltage plateau is attributed to the preferential oxidation of the plated lithium which is also known as the stripping process, due to its lower standard electrode potential in comparison to

the lithium intercalated into the graphite[53]. Smart et al [68] and Ratnakumar et al [69] use this technique for the detection of lithium plating in their study.

The most commonly used detection technique for the detection of the reversibility of lithium plating is the observation of high voltage plateau during the subsequent discharge phase after the charging phase that induced the lithium plating on the surface of the anode [63]. This technique is regarded as a semi-quantitative or a fully quantitative for the evaluation of the reversibility of lithium plating.

A recent study by Campbell et al. [97] has demonstrated the difficulty in de-coupling the influences of plating re-intercalation, cell self-heating, and solid-state concentration gradients on the observation of the high voltage plateau. Furthermore, a study by X-G. Yang et al. [98] suggest that when the cell is immediately discharged after charging, the use of the plateau length for quantification of lithium plating may greatly underestimate the amount of plating since re-intercalation into graphite could still occur even as the current is being drawn from the cell. Uhlmann et al. [78] and S. Schindler et al. [99] uses an alternative to the discharge plateau technique is to detect the voltage plateau during a rest phase following charging. Since the cell is in an open circuit and no current is allowed to flow in the external circuit, all stripped lithium is re-intercalated into graphite.

2.5 Reversibility of Lithium Plating and its detection

In the event of lithium plating, it is also possible that a part of the plating is recovered as active material during a subsequent discharge or due to the intercalation of plated lithium into the graphite on a subsequent rest period. The recovery of plated lithium on a subsequent discharge is possible because the oxidation of the plated lithium is easier than the deintercalation of lithium from the graphite [28][100]. Some researchers have also hypothesized that the plated lithium on the surface of the anode chemically re-intercalates into the graphite given a sufficient amount of time [25], [64], [101].

In the event of lithium plating during the charging of the cell, the reversible and irreversible part of the plated lithium cannot be distinguished. It is only after the subsequent discharge phase, that we have a qualitative understanding of how much of the plating underwent reversibility. There are

two processes that it is taking place simultaneously during the subsequent discharge phase: the re-intercalation (could be electrochemical or chemical) of plated lithium into the graphite and the migration of lithium ions to the cathode. During this discharging phase, the actual loss of lithium inventory happens when the plated lithium becomes electrically isolated from the graphite electrode which is also known as the "Dead Lithium" [16].

M. Petzl and M.A. Danzer [57] proposed a model for lithium plating and stripping processes and how it is influenced by the State of Charge as illustrated in Fig 2.6.

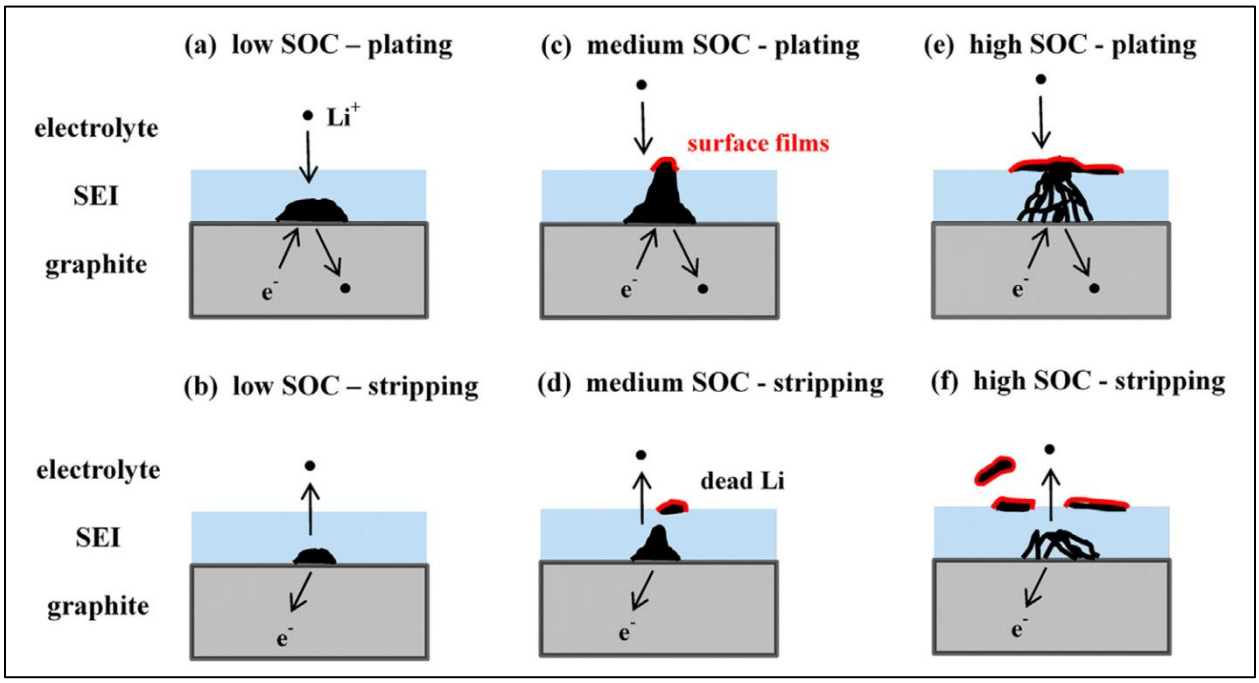

Fig 2.6: Simplified model of the lithium plating-stripping process at different SOC levels: (a) plating and (b) stripping at low SOC; (c) plating and (d) stripping at medium SOC; (e) plating and (f) stripping at high SOC [57]

At the lower state of charge, a significant amount of plating occurs in a small amount of time and the characteristic of this plating is usually dense and thick. The dense nature of plating is observed within a limited distance from the anode and lies within the envelope of the protective SEI layer. On subsequent discharge, most of the plated lithium is stripped. At medium states of charge, the plated lithium grows through the SEI layer and gets in contact with the electrolyte leading to the formation of surface films. Lithium inventory is now lost in the formation of

surface films as well as due to the electrical isolation of lithium in the form of dead lithium. At higher states of charge, lithium plating is more dispersed due to low charge currents and it leads to the formation of fragile dendrites that aren't dense and are susceptible to electrical isolation. Consequently, a higher amount of lithium inventory is lost due to surface film formation and electrical detachment during the subsequent discharge phase. Thus, at higher SOC there is an increase in the amount of irreversible plating.

J. Wandt et al. [42] used operando EPR spectroscopy for quantifying the percentages of dead lithium and lithium used in the SEI layer formation. Lithium plating was induced in an overcharged condition which ensured no re-intercalation i.e. the applied current was divided into a plating current and an SEI layer formation current. During the discharging of the cell, the entire discharging current could be regarded as the stripping current. Comparison of the slopes of the EPR amplitude due to these currents the efficiencies for dead lithium, SEI layer formation, and stripping was calculated and verified against the Coulombic Efficiency obtained from the electrochemical data.

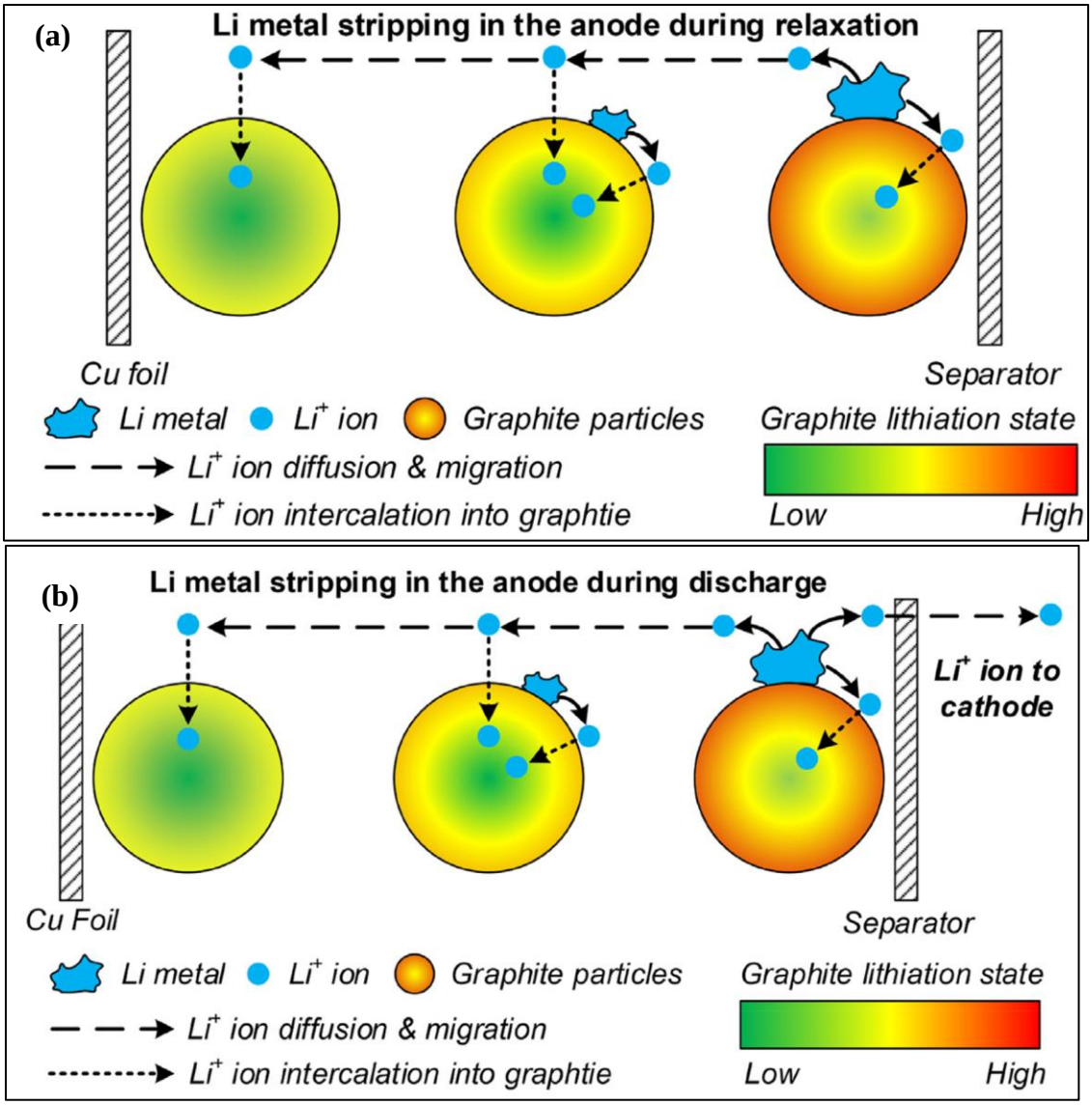

Fig 2.7: Schematic illustrating the differences between the stripping reaction in case of Lithium plating followed by a: (a). Relaxation phase; (b). De-lithiation phase [98]

X.G. Yang et al. [98] illustrates with a schematic the differences between the stripping reaction during a subsequent relaxation phase and a subsequent de-lithiation phase after lithium plating has been induced. As illustrated in Fig 2.7 (a) the rate of intercalation at the separator interphase is limited which leads to the formation of Li^+ ions that migrate towards the Cu foil. Thus, during the relaxation phase, the Li^+ ions near the separator have two possible destinations: local intercalation into graphite and moving towards the Cu foil in the form of electrochemical stripping. However, in the case of Li metal stripping during the de-lithiation phase as shown in

Fig 2.7 (b), the Li^+ ions have three possible destinations: local intercalation into graphite, migration towards the Cu foil and migration towards the cathode in delivering the output current.

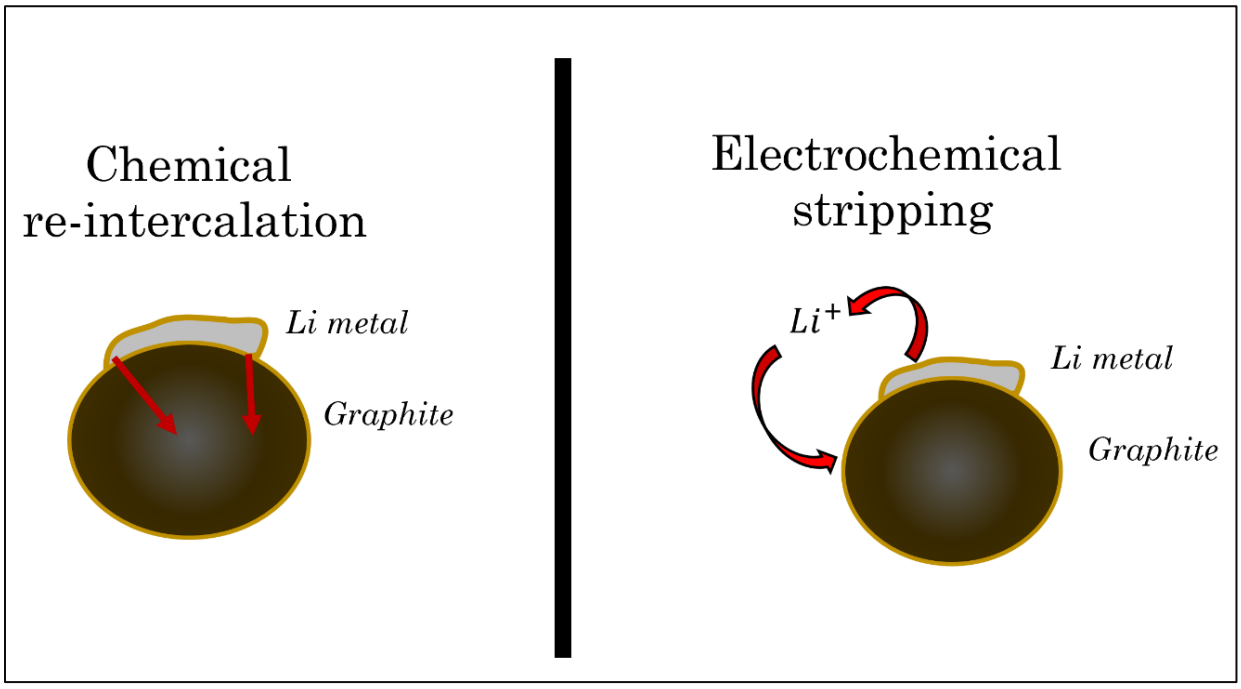

Fig 2.7: Schematic of the two techniques in which plated lithium can be re-intercalated

As discussed earlier, there are two factors promoting the reversibility of lithium plating, Li ions re-intercalation or shuttling back to the cathode. In the event of a long rest phase after the charging of the cell, plated lithium could re-intercalate into the graphite. There are two ways in which we believe this re-intercalation happens:

a) Chemical Re-intercalation: In this process, the plated lithium metal diffuses into the graphite through the process of solid-state diffusion. This process is driven by the concentration gradients which slowly relaxes upon a considerable time period. The time scale for this process is significantly higher. In this process, lithium disappears from the lower region of the metal chunk as illustrated in Fig 2.7.

b) Electrochemical Stripping: As the anode potential returns above 0.0V during the relaxation, the plated lithium is oxidized to Li^+ according to this reaction:

$$Li \rightarrow Li^{+} + e^{-}$$ Equation 2.3

This frees up an electron that is free to reduce and intercalate a Li^{+} ion at a new location which is driven by the local potential difference between graphite particles. Through the work done in this thesis, we attempt to further investigate the fundamentals behind the reversibility of lithium plating in order to devise strategies to mitigate long-term damage to the cell if lithium plating has been detected.

CHAPTER 3 – SINGLE DISCHARGE TESTS

3.1 Introduction

Graphite anodes are susceptible to lithium plating under low temperature and fast charging conditions. In this work, we attempt to study the reversibility of lithium plating. Lithium plating can be induced om the surface of the graphite in two ways: by charging at high rates and/or low temperatures (transport limited) or by charging at a low rate beyond the intercalation limit of graphite (kinetically limited). Differences are expected in these two forms of plating. While transport limited plating tends to accumulate at the anode/separator interface, kinetically limited plating occurs more homogenously on the surface of the graphite. Furthermore, since lithium plating initiates between the graphite surface and the primary SEI layer, small amounts of kinetically limited plating could remain beneath and protected by the primary SEI, while transport limited plating likely ruptures the SEI and exposes plated lithium to reaction with electrolyte. These differences in electrodeposition characteristics could manifest as a significant difference in the reversibility of the plating. It has also been suggested that allowing for chemical re-intercalation through an extended CV phase or adding a rest phase between the charge and discharge could lead to electrical isolation of plated lithium and increase the amount of dead lithium, further reducing reversibility[57].

3.2 Objectives

1. To elucidate the interactions between lithium plating and SEI affecting the reversibility of lithium plating by studying the key differences between high-rate lithium plating induced by transport limitations vs. overcharge plating induced by kinetic limitations.
2. To determine the impact of chemical re-intercalation on lithium plating reversibility by studying the impact of allowing a rest phase after charge vs. immediately discharging.

3.3 Methodology

3.3.1 Fabrication of Coin Cell

The accuracy of results is highly dependent on the quality of the cells that are being used for experiments and maintaining consistency throughout the process. Hence, it is very crucial to be meticulous when it comes to the process of fabricating cells. Lithium is highly reactive in the presence of Oxygen. Hence, the fabrication and the destructive physical analysis of the cell is always done in a hermetically sealed chamber. The fabrication of the coin cell for this study was done in an M-Braun argon-filled Glovebox.

Fig 3.1: M-Braun Glovebox used to conduct coin cell fabrication, destructive physical analysis, and Optical Microscopy

We make sure that we have all the coin cell parts required to fabricate a cell. In this study, Lithium-Graphite half cells are constructed in standard CR2300 coin cells. For a Lithium-Graphite Half-cell, the working electrode is the anode that is punched from a sheet of commercially available MTI Graphite sheet that had a thickness of 50 μm. This electrode had a composition of 94.5% composite graphite and 5.5% SBR+CMC binder. The counter electrode for the half cell is metallic lithium punched from a Metallic Lithium foil (Sigma Aldrich, 0.75 mm thick). A scalpel is used

to scrape off the oxide layer from the surface of the Lithium on both sides of the ribbon before it is punched. This ensures that the layer of freshly available lithium is exposed. Both the graphite electrode and the Lithium counter electrode were punched into 9/16" disks.

The case is taken and placed on a weigh-boat. The graphite electrode is taken and placed at the center of the case. 7-8 drops of EC: EMC (3:7 wt%) with 1.2M $LiPF_6$ electrolyte are added to make sure that the surface of the electrode is sufficiently wetted. A 3/4" inch Celgard 2500 Polypropylene (PP) separator (25 μm) is taken and placed on the graphite electrode. The separator is greater than the graphite electrode in diameter and it covers up the entire area of the case. At this point, it is made sure that the placement of the graphite electrode is centered and there are no air bubbles trapped underneath the separator.

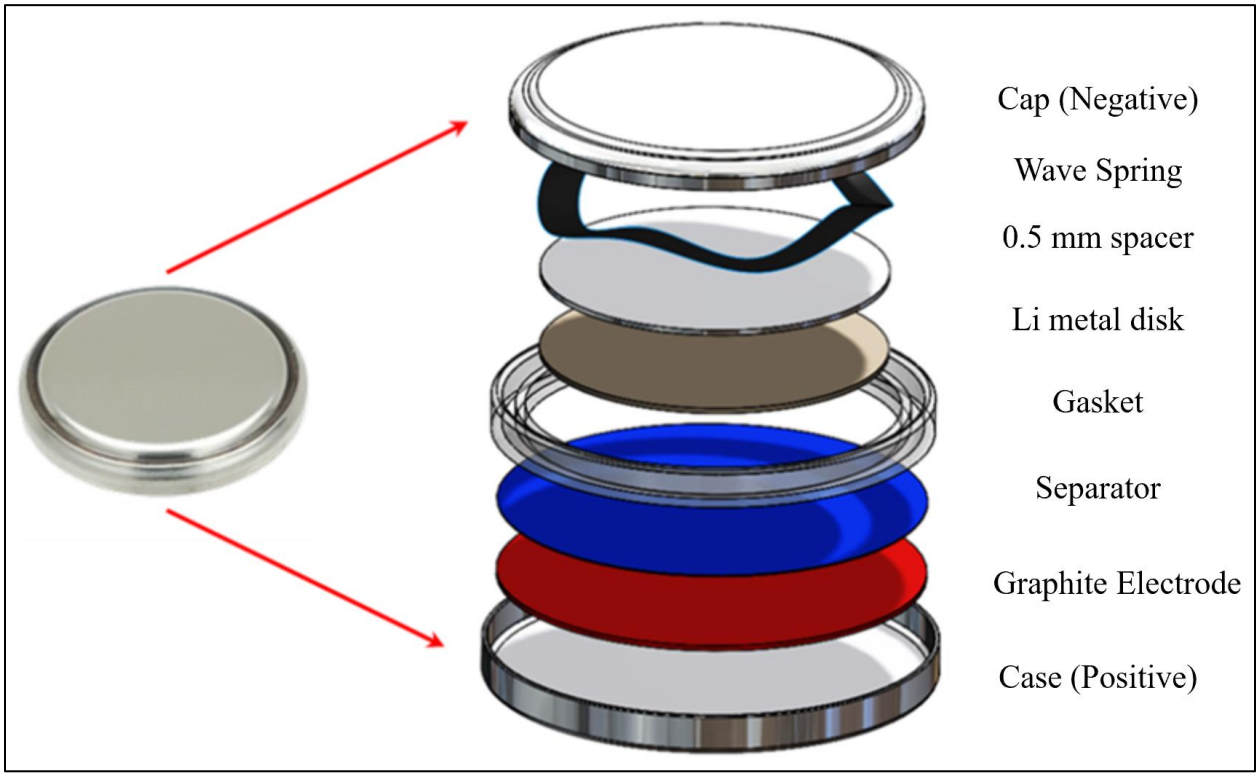

Fig 3.2: Schematic of a Li-Graphite Half Cell

The gasket is taken and placed along the interior side of the rim of the case. 3-4 drops of electrolyte are further added to make sure that the other side of the separator is also wet. The Lithium counter electrode is taken, and it is placed on a Stainless Steel spacer. The Lithium sticks onto the surface

of the spacer quite easily since we scrape the surface of the Lithium electrode before punching it. The electrode-spacer unit is now placed on the wet separator surface with the lithium facing downwards to the separator. The wave spring is now placed on the top of the spacer. 2 more drops of electrolyte are added to make sure that the cell is flooded with electrolyte. This is done to ensure that the results obtained from the cell aren't influenced by electrolyte starvation. The cap is placed on the rim of the gasket and pressed tight. The whole setup is now taken to MTI hydraulic crimper and crimped at a pressure of 750 psi to make sure that the cell is sealed. The cell is cleaned with Isopropyl Alcohol making sure that there are no remnants of electrolytes on its external surface. The cell is now taken out and it could be used for testing.

3.3.2 Experimental Apparatus

Lithium-graphite half cells were used to carry out these experiments. The cells were fabricated in the M-Braun Glovebox as discussed. Lithium is highly reactive to oxygen and moisture in the atmosphere which is why an inert environment is required for the fabrication of cells. The Argon filled Glovebox as shown in Fig 3.1 provides the inert environment for the successful fabrication and Destructive physical analysis of lithium-ion cells.

Fig 3.3: Arbin Battery Tester used for electrochemical testing

Thereafter the Arbin Battery Tester was used to perform the Formation Cycle of the cell and subsequent electrochemical testing. The formation cycle comprises of 2 constant current charge-discharge cycles at a C-rate of C/20 between the voltage cutoff of 0.00V and 2.00V. This step is essential for the formation of the first protective layer of SEI. The Arbin Battery Tester has 16 channels which operate between the voltage window of -5V to 5V and could supply current in the range of 1 mA to 5 A. This device comes with the feature of measuring temperature and internal resistance data along with the usual electrochemical data

Fig 3.4: MTI BTS8-3 coin cell cycler used for Electrochemical Testing

For experiments where precise temperature conditions had to be maintained, the electrochemical testing was done in the MTI BTS8-3 coin cell cycler as shown in Fig 3.4. There are 8 channels available in this device for electrochemical testing. The MTI BTS8-3 coin cell cycler was connected to a novel setup designed to perform temperature controlled studies.

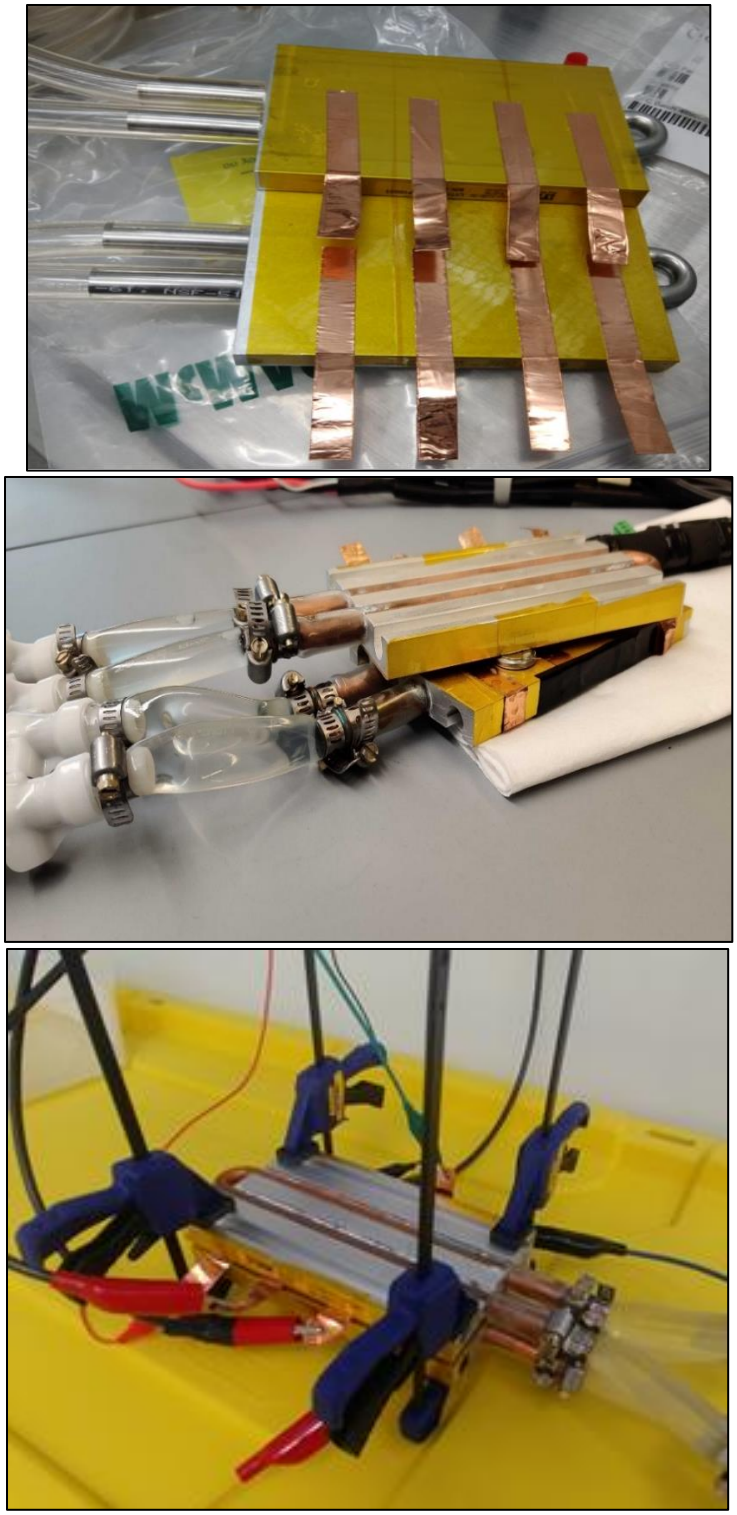

Fig 3.5: Heat exchanger plates used for temperature-controlled electrochemical testing

Fig 3.5 shows a sequential order in which the setup was built. In this apparatus, there are two heat exchanger plates made up of aluminum. A hollow copper tube is fitted on the Aluminum plates which are further connected by hoses to a chiller, through which coolant (50-50 mixture of Ethylene Glycol and Water) is circulated. Copper strips are added which act as the medium of electrical conductivity from the MTI Battery Tester to the positive and negative terminals of the coin cell. The coin cells were sandwiched between the two plates and clamps were fitted on the sandwiched plates to ensure that the cell is in proper contact with the aluminum plates. The chiller maintains the coolant at a specified temperature. The circulation of the coolant at a high flow rate through the hollow copper tube acts as a liquid cooling system that draws away heat from the Aluminum plate through the mode of conduction. The conductive heat transfer in this apparatus is superior due to the high thermal conductivity of Aluminum and isothermal conditions are achieved on the Aluminum plates. 3 hours of liquid cooling through this apparatus was done prior to electrochemical testing to ensure that steady-state conductive heat transfer is achieved, and the coin cell has reached an isothermal state.

3.3.3 Electrochemical Testing

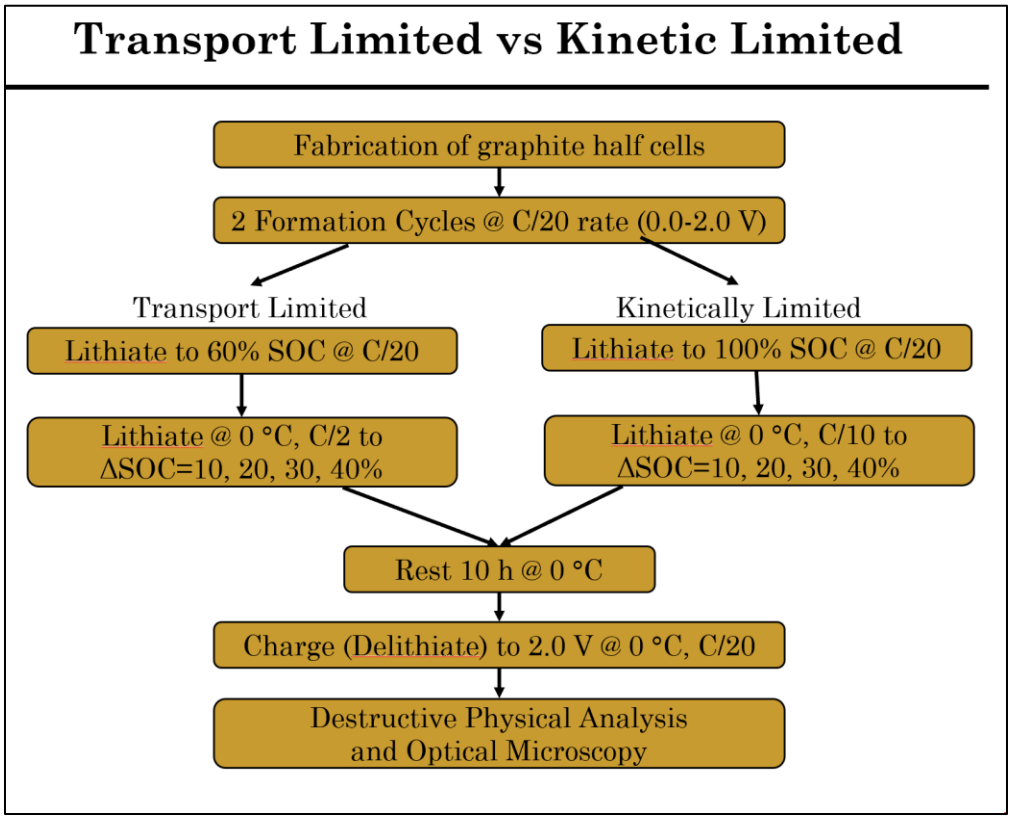

Fig 3.6: Schematic of electrochemical testing protocol followed to illustrate the difference between Transport Limited and Kinetic Limited Lithium plating

In order to develop a fundamental understanding of the irreversible processes associated with lithium plating, two different strategies were devised to reliably induce lithium plating. Plating can be caused by either mass transport limitations under high rate or low-temperature conditions, or by kinetic limitations due to overcharge of the graphite material.

For the case of transport limited plating, cells were initially lithiated at C/20 rate at ambient temperature up to 60% SOC. This starting condition was chosen based on a previous study by Uhlmann *et al.*[78], which successfully induced lithium plating under similar conditions. Since the rate of solid-state diffusion in graphite is known to decrease drastically at high SOCs, it is most likely that plating will occur after the transition to the third plateau of graphite. After 60% SOC, discharge pulses of ΔSOC=10, 20, 30, or 40% were performed at 0 °C at a C/2 rate.

To study kinetically limited plating, cells were initially lithiated at C/20 rate at ambient temperature up to 100% SOC. This starting condition ensures that there are no vacancies remaining

in the graphite layered structure. Therefore, all charge is expected to contribute to the lithium plating reaction. The discharge pulses were again applied to ΔSOC=10, 20, 30, or 40% but were performed in this case at 0 °C at a C/10 rate.

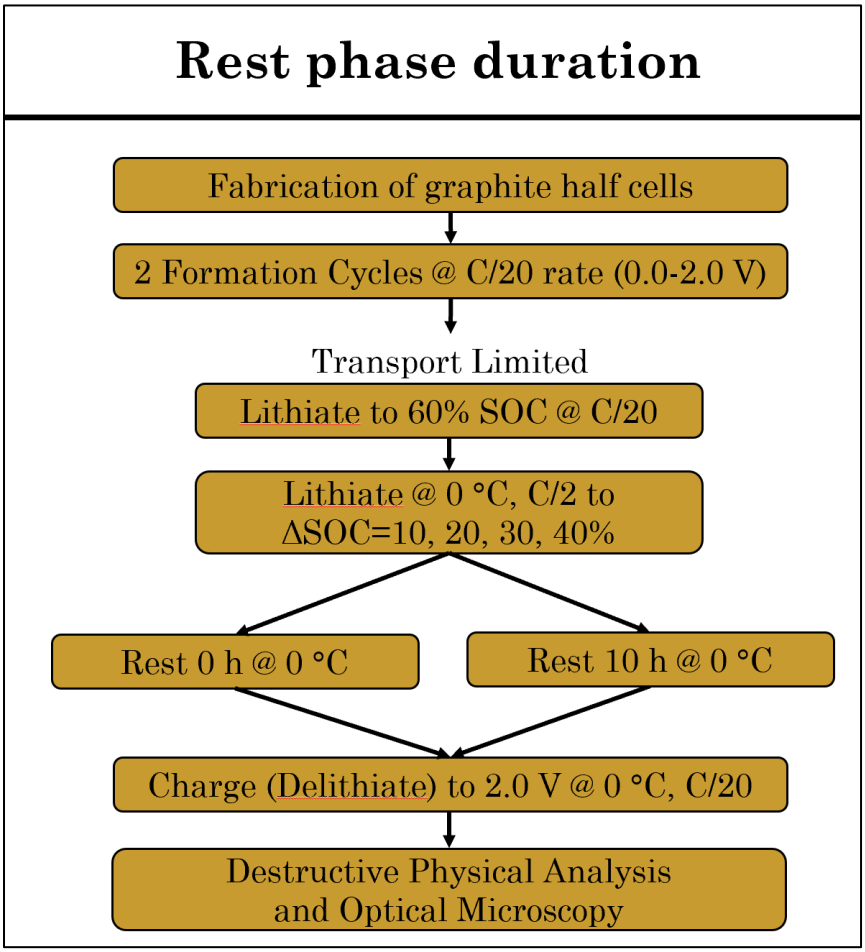

Fig 3.7: Schematic of electrochemical testing protocol followed to illustrate the effect of rest phase duration on the reversibility of lithium plating

The next objective was to study the effect of the duration of the rest period on the reversibility of plating. As seen from Fig 3.7 the transport limited cases were taken for consistency with the previous set of experiments. The Li-graphite half cells were lithiated till 60% SOC at a low C-rate of C/20. Thereafter, a high C-rate of C/2 was chosen to lithiate the cells further to different levels of SOC which was designed to facilitate transport limited plating. At this point, one set of cells was left to rest for 10 hours at 0 °C followed by de-lithiation at a slow rate of C/20. The other set

of cells was immediately de-lithiated at the slow rate of C/20. After the de-lithiation, the cells were disassembled in the M-Braun Glovebox for optical microscopy.

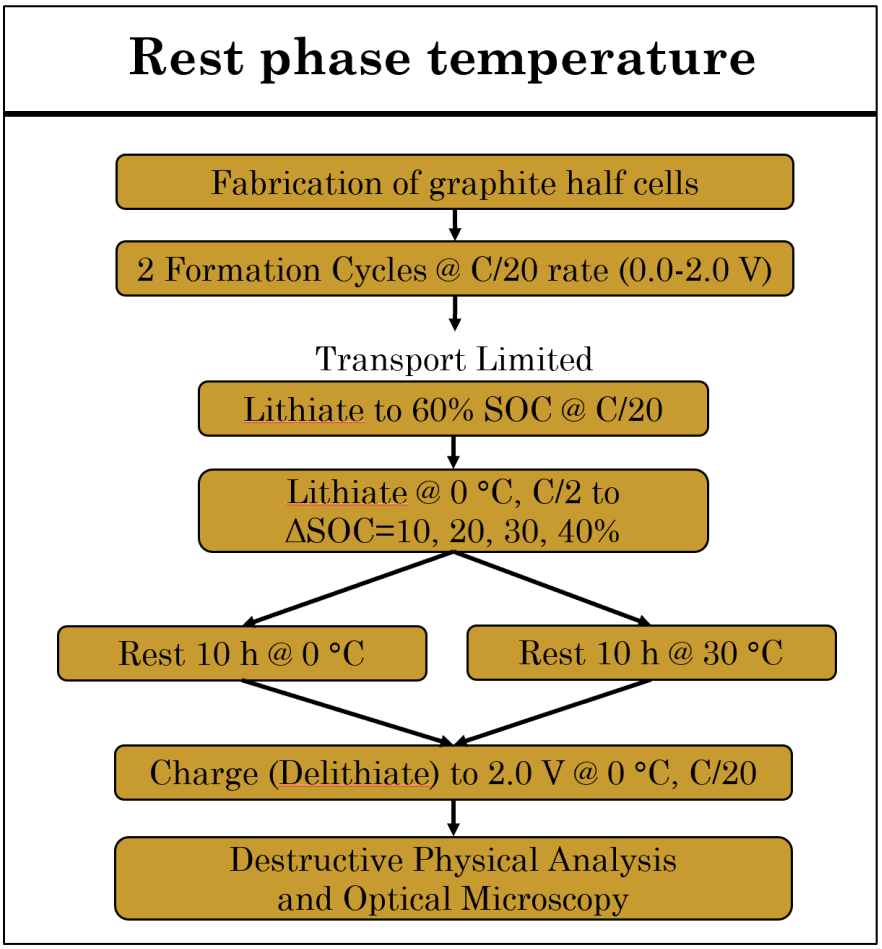

Fig 3.8: Schematic of electrochemical testing protocol followed to illustrate the effect of temperature during the rest phase on the reversibility of lithium plating

The effect of temperature during the rest phase was an interesting aspect to be explored. Low temperatures would impede the chemical kinetics and slow down the re-intercalation but on the other hand, higher temperatures would promote the rate of SEI growth. In order to explore the effect of temperature, a wide range of temperatures (0°C and 30°C) was chosen. As seen from Fig 3.8 the transport limited cases were taken for consistency with the previous set of experiments. The Li-graphite half cells were lithiated till 60% SOC at a low C-rate of C/20. Thereafter, a high C-rate of C/2 was chosen to lithiate the cells further to different levels of SOC which was designed to facilitate transport limited plating. This high-rate lithiation was followed by a relaxation phase

of 10 hours at two different temperatures (0°C and 30°C). The cells were then de-lithiated at a slow rate of C/20 before disassembly and followed by optical microscopy

3.3.4 Destructive Physical Analysis

Fig 3.9: Leica Si9 optical microscope used for Postmortem Analysis

Electrochemical testing was followed by a destructive physical analysis in order to examine the graphite electrode. The cell was carefully disassembled in the M-Braun Glovebox so that the graphite electrode doesn't react with the environment leading to the altering of the appearance. Electrical tape was stuck on one side of the coin cell before the disassembly to avoid the external shorting of the cell. The disassembly was carried out using pliers and tweezers. The graphite electrode was carefully extracted and placed under the lens of the microscope for visual analysis.

3.4 Results and Discussion

3.4.1 Transport Limited vs Kinetic Limited

Discharge Voltage

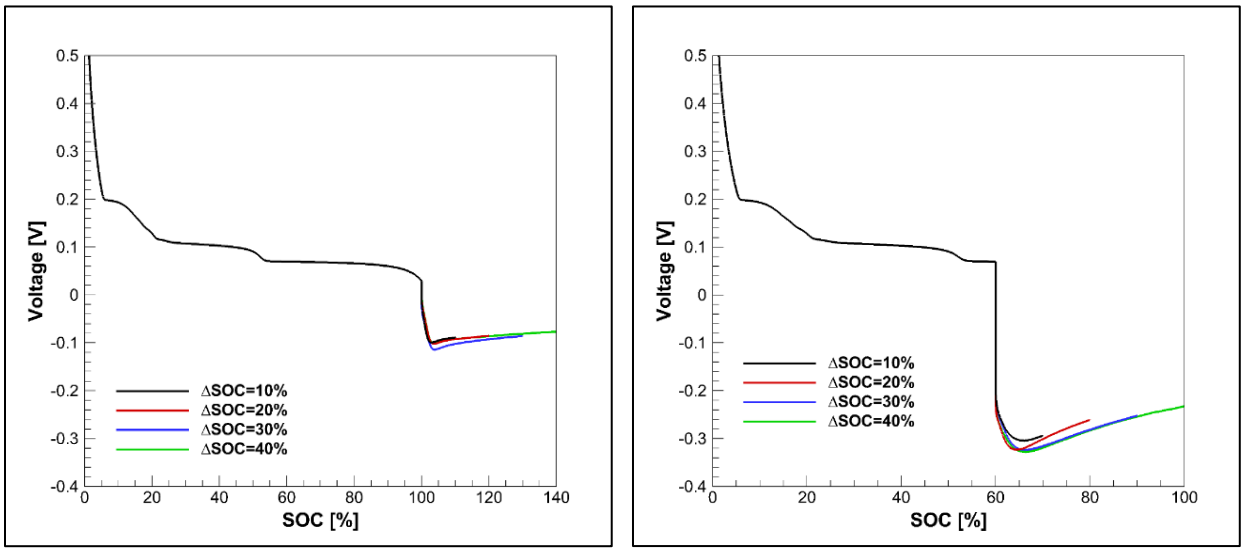

Fig 3.10: The voltage profiles of cells under transport limited and kinetically limited charging profiles are compared. In transport limited (a), graphite was lithiated to 60% SOC at C/20 rate and ambient temperature before applying C/2 pulses at 0 °C. In kinetically limited (b), graphite was lithiated to 100% SOC before applying C/10 pulses at 0 °C.

Fig 3.10 demonstrates the discharge protocols used to study (a) transport limited plating and (b) kinetically limited plating. In each case, the voltage curve reaches a minimum within 5% SOC of the onset of the plating pulse, indicating that the nucleation barrier for the onset of lithium plating has been overcome. For transport limited plating, lithium plating tends to nucleate at defect sites or locations of low active material content, which experience high local current density and local overcharge. Lithium deposits are most likely to occur at the anode-separator interface under transport limited conditions since the use of electrolytes with non-unity transference numbers inevitably results in the development of electrolyte concentration and potential gradients. The electrolyte concentration and potential both reach their maximum within the anode at the anode-separator interface, making the localized reaction more favorable. The minimum in the voltage curve represents a transition from plating hotspots to a film-like plating regime. The increase in cell voltage corresponds to an increase in the active area for the lithium plating reaction, which

results in a decrease in overpotential for the cell. After the voltage minimum, the majority of the total current contributes to the lithium plating reaction.

In the case of kinetically limited plating, a small nucleation overpotential is observed before the cell voltage slightly increases with additional capacity. Since a C/10 current is employed, the concentration gradient established in the electrolyte is minimal and current in more uniformly distributed through the depth of the anode. Since the current can only be contributing to the lithium plating reaction when graphite is overcharged, it is expected that the plating deposits will also be distributed more evenly through the electrode depth than in the transport limited cases. The similarity of the voltage curves between cells demonstrates strong repeatability between samples, despite the inherent stochasticity of the lithium plating process.

Relaxation Voltage

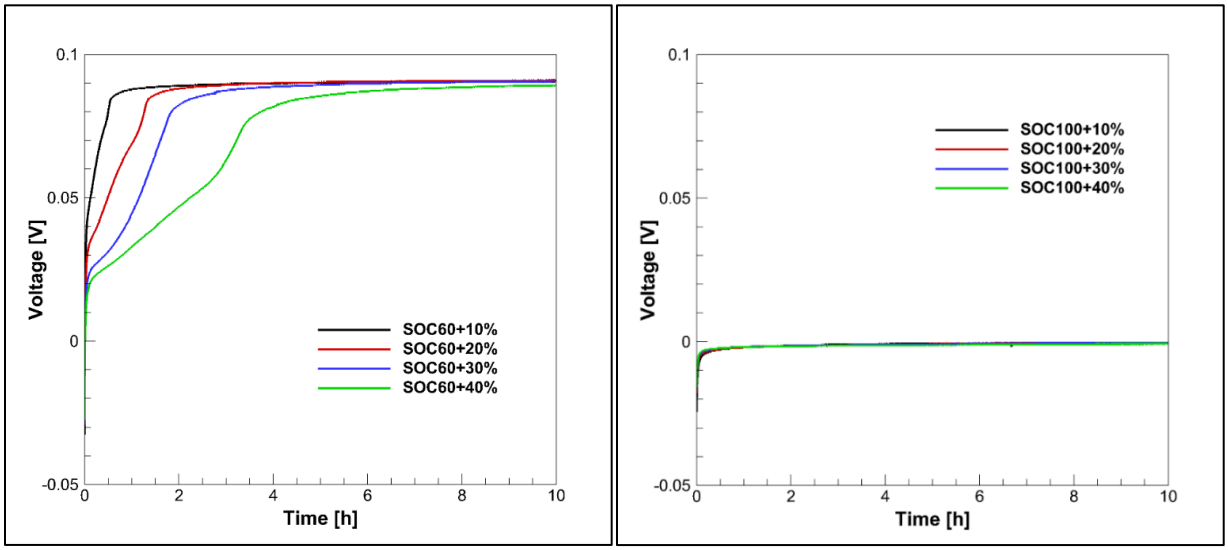

Fig 3.11: The relaxation voltage profiles of cells: a). transport limited, b). kinetically limited

The voltage profiles during the 10 h rest phase following discharge are shown in Fig 3.11. In transport limited plating, the relaxation voltage profiles contain the distinctive plateaus that indicate the electrochemical stripping and re-intercalation of plated lithium. The length of the plateau indicates the extent of lithium stripping. As expected, the amount of lithium stripping increases with increasing amounts of lithium plating.

For all cells that experienced kinetically limited plating, the rest phase voltage profile did not contain a plateau. This is expected since the lack of interstitial site availability is fully charged graphite prevents re-intercalation from occurring. Notably, it was found that the voltage at open circuit returns to a value of 0.0 V vs. Li/Li+ when overcharge plating has occurred. This observation could present an alternative detection method for lithium plating in overcharged cells. Furthermore, the distinct difference in relaxation behavior highlights the importance of understanding the fundamental differences between the two methods of inducing plating.

Charge Voltage

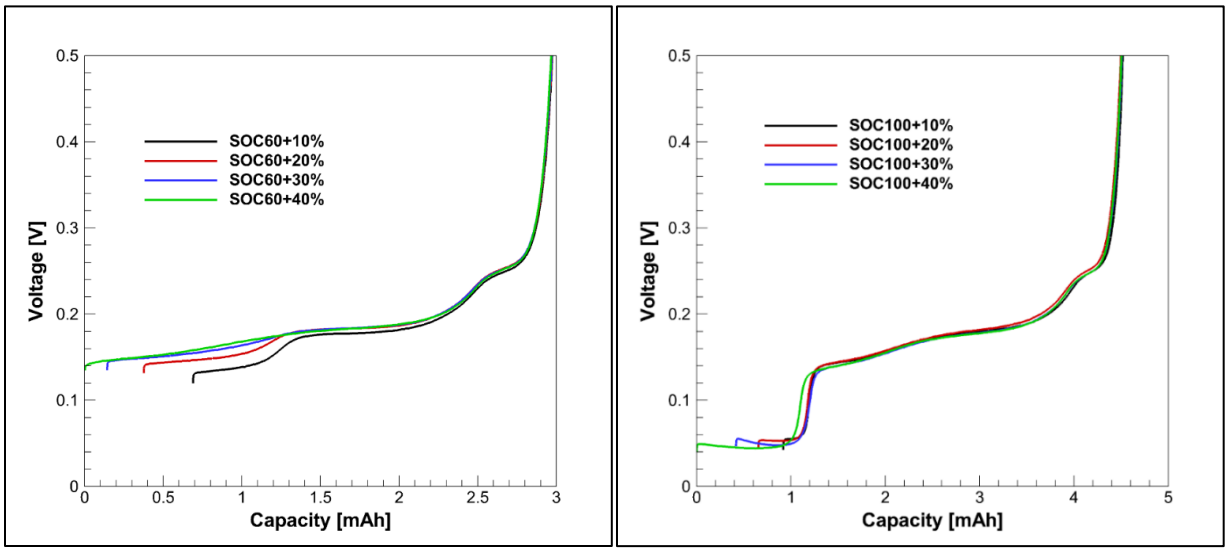

Fig 3.12: The charge voltage profiles of cells: a). transport limited, b). kinetically limited

The voltage profiles during the charge phase in the transport and kinetically limited cells are shown in Fig 3.12. All curves are shifted to end at the same capacity value so that the characteristics of their shapes can be compared. In the transport limited cases, the main difference between cases is the smoothening of the low voltage plateau with increasing ΔSOC. A loss of definition in the plateaus is an *in-situ* indicator of overshooting phases. There are two possible factors contributing to this behavior. Firstly, since the charge was performed at 0 °C, the slow solid-state diffusion of graphite at this temperature could be limiting the rate of stage 1 dissolution and introducing stage 2L before it is thermodynamically expected. Additionally, it could be caused by mass transport limitations in the electrolyte as a result of pore-clogging due to lithium plating. This would result in difficulty discharging the graphite further in the depth of the electrode and cause the particles near the separator interface to discharge at a higher rate than those near the current collector. In

order to de-couple the contributions of these two effects, it would be necessary to perform a control test in which cycling was performed at 0 °C at C/20 rate, where no lithium plating is expected to occur.

Under kinetically limited conditions, the voltage profile during charge is shown in Figure 3.12 (b). An additional plateau is observed at the start of de-lithiation, which corresponds to the stripping of plated lithium. Due to the low potential of the lithium stripping reaction, stripping occurs prior to the de-intercalation of lithium from the graphite. A slight overpotential is required to initiate stripping in the ΔSOC=30 and 40% cases, which may be related to the formation of SEI due to the reaction of metallic lithium with the electrolyte.

Post-Mortem Analysis Results

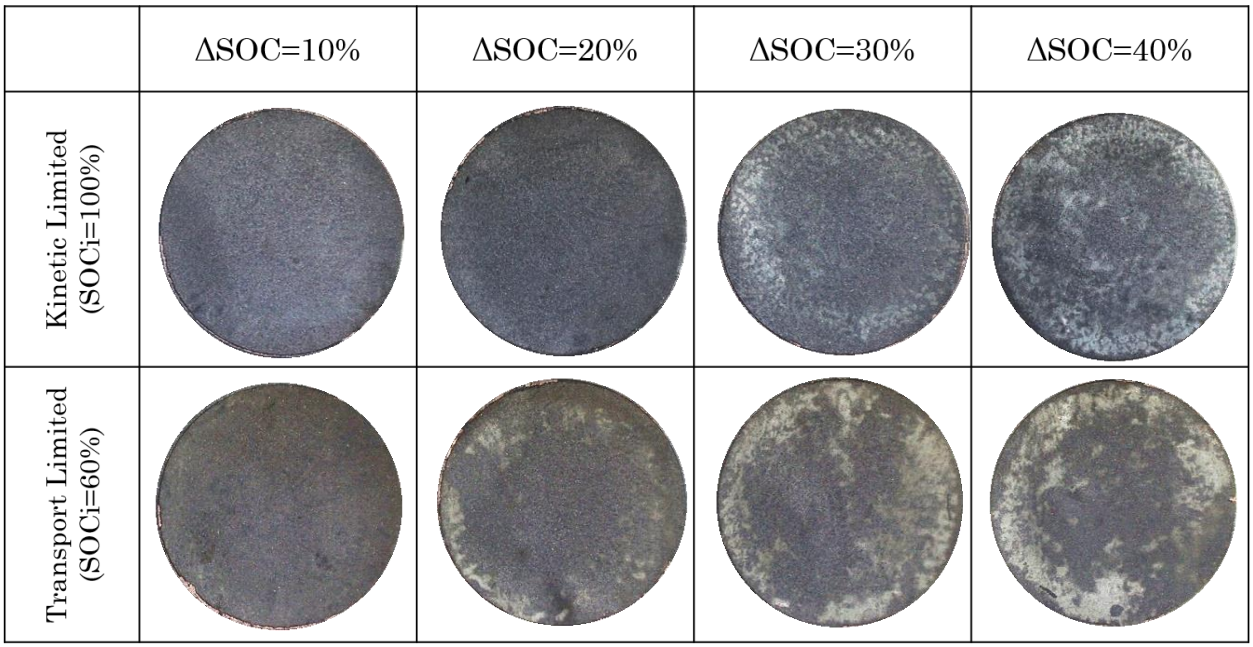

Fig 3.13: A comparison of the postmortem analysis of the different transport limited and kinetically limited cases by optical microscopy at 0.6x magnification.

Based on the model of Petzl and Danzer [57], we expected that both types of plating would initially form small deposits between the graphite surface and the native SEI layer on the graphite. With enough plating, these deposits would grow large enough to rupture the SEI layer and expose the lithium metal to the electrolyte, where it would react and reduce the reversibility of the

plating/stripping reaction. The model of Petzl and Danzer [57] also predicts that plating would spread in a film-like fashion after rupturing the SEI, which suggests that the SEI rupture occurs at or shortly after the voltage minimum.

The post-mortem images of the graphite electrodes after undergoing either transport or kinetically limited plating are shown in Fig 3.13. It was hypothesized that under transport limited conditions, the plating would be more localized near the anode-separator interface (top surface in the pictures) and that the more localized plating current density would lead to faster rupture of the primary SEI layer and thus the early onset of film-like lithium plating. In contrast, the kinetically limited plating was expected to occur more uniformly throughout the electrode depth. Since the current would be distributed more evenly across many lithium deposits, the SEI rupture would be delayed and the overcharge plating was expected to demonstrate a higher degree of reversibility.

From Figure 3.13, it is evident that film-like plating onset at an earlier SOC in the transport limited case than in kinetically limited. At ΔSOC=10%, no lithium deposits are visible, suggesting that the extent of plating in each condition was minimal enough to prevent SEI rupture. However, at ΔSOC=20%, significant amounts of lithium metal were visible in the transport limited cells, while no deposits large enough to view with optical microscopy occurred in the kinetically limited cells. The film-like plating becomes visible in kinetically limited plating only at ΔSOC=30 and 40%, representing extreme overcharge conditions. Even after becoming visible, the kinetically limited plating looks much patchier, as though it had initiated at many sources and the growths had just started to spatially overlap. The transport limited cases contain denser plating deposits, suggesting they initiated at fewer locations and spread across the electrode surface as a film.

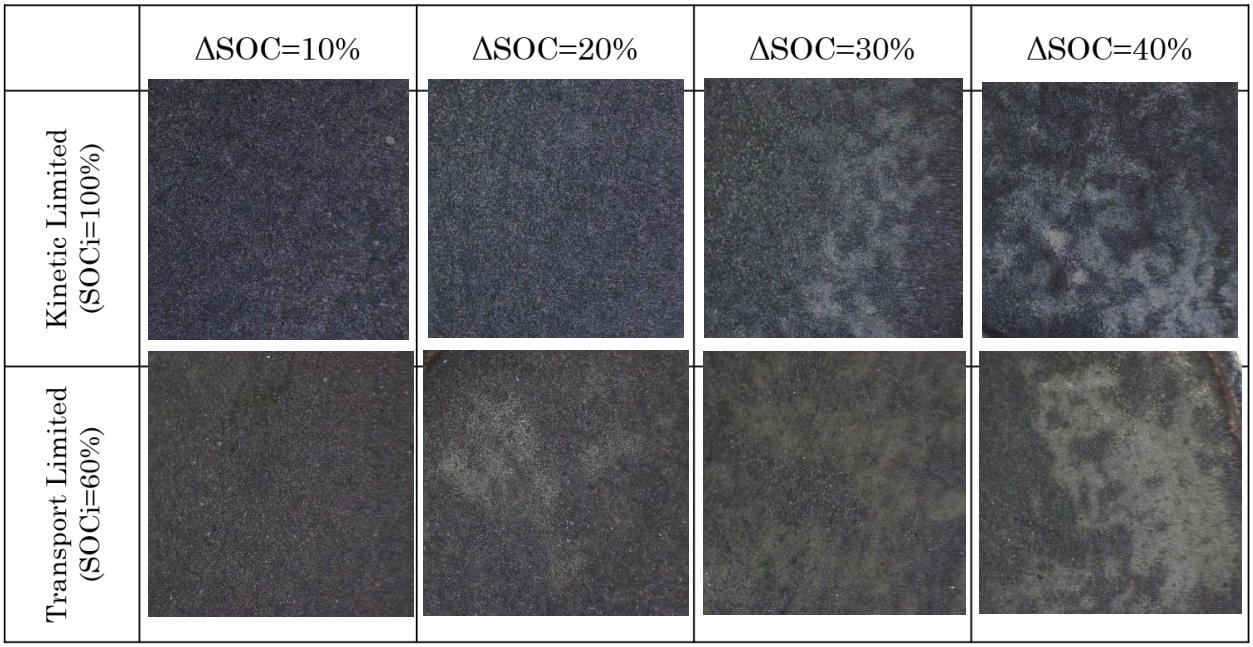

Fig 3.14: A comparison of the postmortem analysis of the different transport limited and kinetically limited cases by optical microscopy at 30x magnification.

Images obtained from optical microscopy at 30x magnification of the same electrodes are shown in Fig 3.14. Still, no deposits are visible at ΔSOC=10%, while the difference in the onset point of film-like plating is evident at ΔSOC=20%. The variation in plating morphology is confirmed in the ΔSOC=30 and 40% cases, with the transport limited cells showing more connectivity in the plating deposits and the kinetically limited cells showing more loosely connected patches of lithium plating.

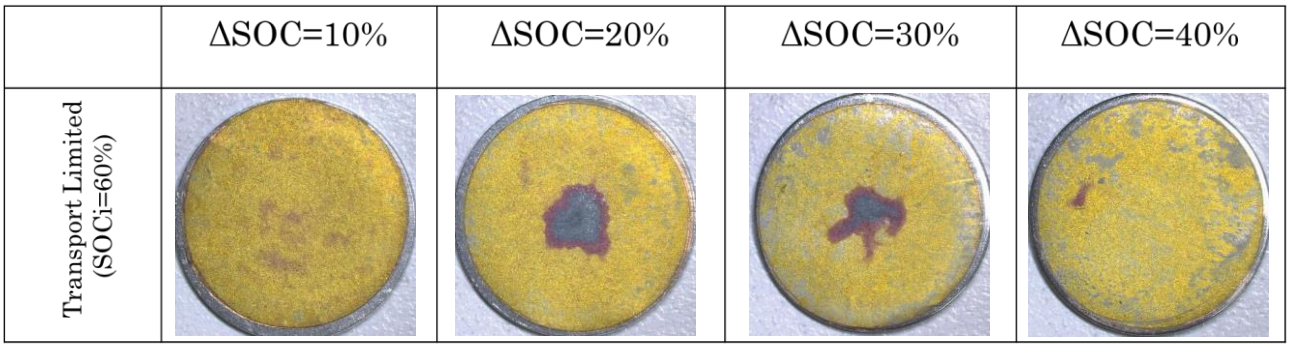

Fig 3.15: A comparison of the postmortem analysis of the different transport limited cases in the lithiated state by optical microscopy at 6x magnification.

It is also interesting to note that a second plateau occurs at higher potential during the rest phase in each of these cells, as seen in Fig 3.11(a). Since the final SOC of all these cells lies on the third plateau of graphite, it is expected from the analysis of Bauer *et al.* [43], [44] that the equilibrium phases are gold stage 1 and red stage 2 graphite. However, in the cells opened in the fully lithiated state, the presence of some blue stage 2L was identified, as shown in Fig 3.15. We believe that the second plateau appears due to the concurrent dissolution of the stage 2L and stage 1 phases and the formation of more stage 2.

Coulombic Inefficiency

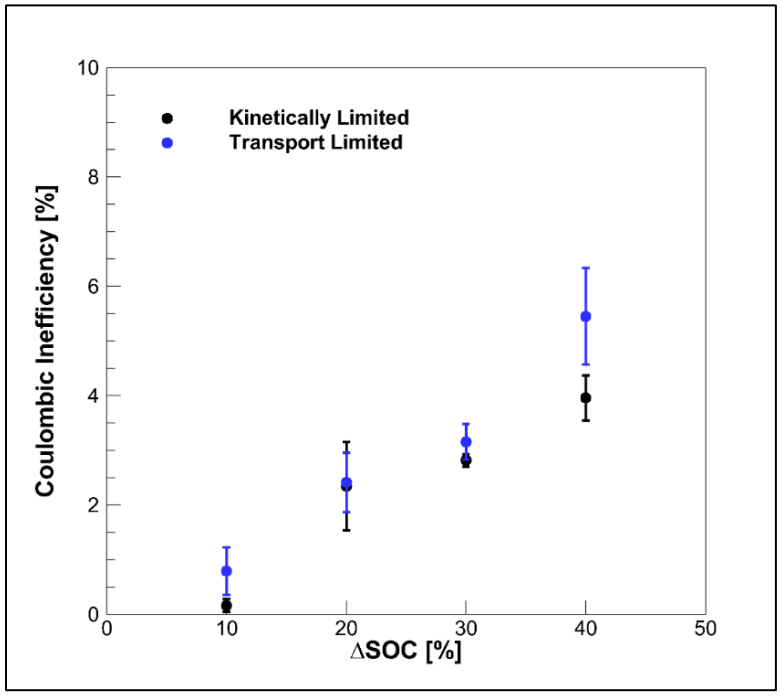

Fig 3.16: A comparison of the Coulombic inefficiencies of the different transport limited and kinetically limited cases after one cycle.

The Coulombic inefficiency (CI) of cells undergoing plating to various extents under transport and kinetically limited conditions is shown in Fig 3.16. The CI was evaluated as the complement of the ratio of charge capacity to discharge capacity. Major contributors to the inefficiency of cells with lithium plating include the formation of secondary SEI when lithium metal contacts the electrolyte and the formation of electrically isolated "dead" lithium. For all values of ΔSOC, the transport limited cells demonstrated a slightly higher CI. This difference is more evident when it is recognized that all of the current in kinetically limited cells went towards plating, while a portion

of the current in transport limited cases went towards the much more efficient intercalation reaction. This result demonstrates that plating under fast charge scenarios may experience a lower degree of reversibility than under overcharge scenarios. The kinetically limited cells at ΔSOC=10% experienced an average CI of 0.17%, which indicates almost no irreversibilities due to the lithium plating reaction and supports the hypothesis about the primary SEI layer protecting the plating from a reaction. The highest CI measured was 6.1%, when a maximum of 40% of charge passed by the cell was contributed by lithium plating. Therefore, the lower bound on the reversibility of the lithium plating/stripping reaction was about 85% under these conditions.

3.4.2 Effect of the duration of the Rest Phase

Postmortem results

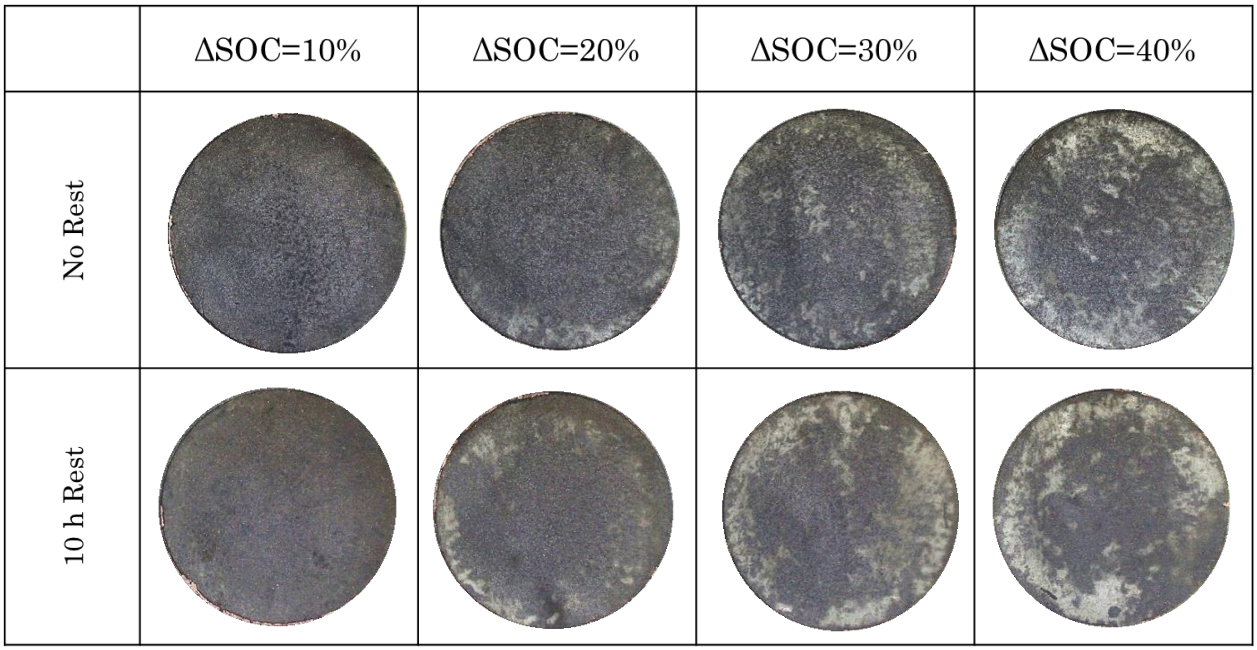

Fig 3.17: A comparison of the postmortem analysis of the cases with no rest vs the cases with 10 hours of rest, by optical microscopy at 0.6x magnification.

From the model of Petzl and Danzer [57], it was predicted that lithium plating would demonstrate a lower degree of reversibility when a 10 h rest was allowed than when the cells were immediately de-lithiated. Petzl and Danzer [57] observed that when they performed CC-CV charging at low temperatures, no re-intercalation plateau was present if the CV phase extended long enough and

the amount of irreversible plating greatly increased for the same case. They explain that chemical re-intercalation can occur during the CV phase if the incoming current flux is low enough. This may cause a loss of electrical connection between the graphite and lithium deposits. We hypothesized that a similar process would occur during the rest phase following a constant current charge, whereby the plated lithium in contact with the graphite surface would chemically re-intercalate and leave a portion of the plated lithium electrically isolated. Therefore, it was expected that the cells given a rest phase before de-lithiation would have a higher CI than those which were discharged immediately.

From the electrode images in Fig 3.17, no distinct difference is identifiable between the electrodes with and without a 10 h rest. Furthermore, the CI values in Figure 3.16 do not indicate a statistically significant difference between the two cases. One possible explanation for the result is that chemical re-intercalation requires more than 10 h to create electrical isolation when the cell is stored at 0 °C. Although this test was inconclusive, future testing will be done to determine the influence of rest time on plating reversibility and determine the proper time scale to observe the effects of chemical re-intercalation.

3.4.3 Effect of Temperature of the Rest phase

Coulombic Inefficiency

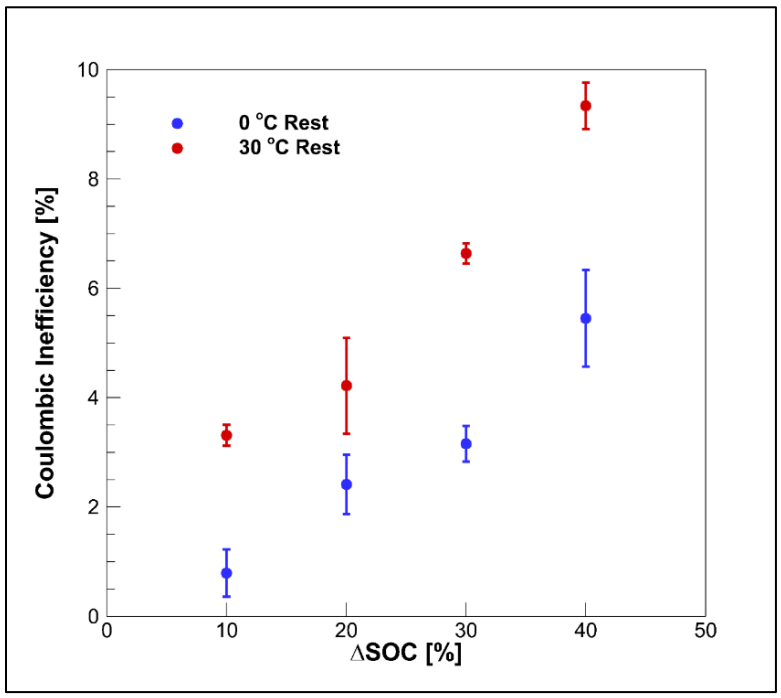

Fig 3.18: A comparison of the Coulombic Inefficiencies of the cases with rest phase temperature of 0°C vs 30°C after one cycle

It is clear from Fig 3.18 that the rest phase temperature was the factor having the most significant influence on the reversibility of the lithium plating process. For each value of ΔSOC, the cell that underwent rest at 30 °C experienced an average Coulombic inefficiency nearly twice as high as the baseline cell rested at 0 °C. For the ΔSOC=40% cells with a 30 °C rest, the average CI of 9.3% yields minimum reversibility of the lithium plating reaction of 23.3% (assuming the worst case in which all of the 40% capacity goes towards lithium plating).

Postmortem Results

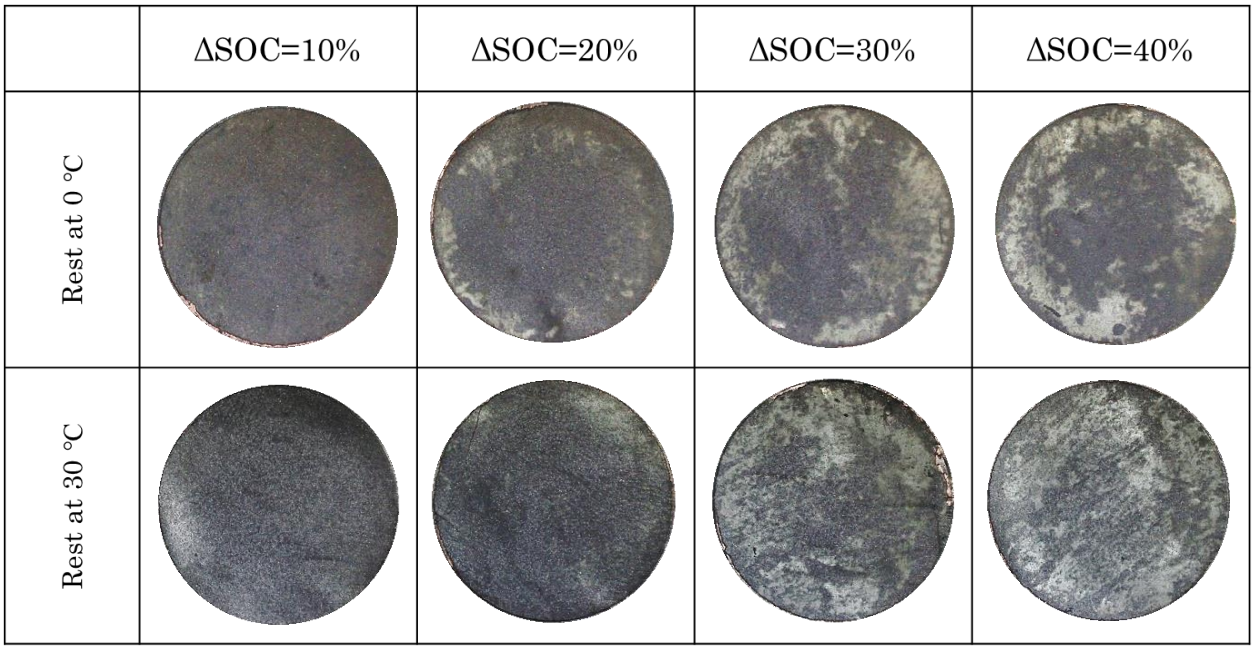

Fig 3.19: A comparison of the postmortem analysis of the cases with rest phase temperature of 0°C vs 30°C, by optical microscopy at 0.6x magnification

The graphite electrode images from the cells which underwent rest at various temperatures are shown in Fig 3.19. The cells that rested at 30 °C show an unexpected change in plating morphology. The lithium plating on these electrodes covers more of the surface and appears more spread out. This suggests that lithium self-diffusion became prominent at 30 °C, allowing atoms to move along the surface. All other rest phase processes are also accelerated at a higher temperature, including the rate of electrochemical stripping, the rate of chemical re-intercalation, and the rate of SEI formation on both the lithium and graphite surfaces. The increased irreversibility can mainly be ascribed to the increase in SEI formation rate and the need for a thicker SEI layer to passivate the surface at a higher temperature. This experiment suggests that the best treatment for recovery of plated lithium may involve storing the cell at low temperature to mitigate the growth of irreversible SEI.

3.5 Conclusion:

The experiments performed in this chapter were intended to elucidate the factors affecting the reversibility of the lithium plating reaction. First, we investigated the differences between plating induced through fast charging (transport limited) and through overcharge (kinetically limited). It was determined that transport limited plating led to an earlier onset of the film-like plating regime since the current was more localized at the electrode-separator interface. In contrast, the cells with kinetically limited plating showed a later onset of film-like plating, suggesting that at low degrees of overcharge, small plating deposits can remain beneath the graphite SEI layer and maintain a high degree of reversibility. Due to the higher Coulombic inefficiency and the connectivity of plating deposits, we conclude that plating induced by fast charging has more potential to cause lasting degradation through pore-clogging and dendrite growth.

An interesting observation from this experiment is that cells containing plating due to kinetic limitations maintain a rest phase potential of about 0.0 V vs. Li/Li^+, while the transport limited cells return to the expected OCP of graphite during the third plateau (~89 mV vs. Li/Li^+). This difference could be useful in identifying an overcharged cell in an unbalanced module since the cell OCV would be expected to deviate from that of surrounding cells. Due to the lack of vacancies in the kinetically limited cells during rest, no re-intercalation plateau is observed in the rest phase voltage profile. Instead, the charge phase contains an initial low-voltage plateau which corresponds to the lithium stripping process and is not observed for the transport limited cases.

The most significant influence on the reversibility of lithium plating was found to be the temperature of the cell during the rest phase. Higher temperatures accelerate the rate of all processes occurring during rest, including electrochemical stripping, SEI formation, lithium self-diffusion, and chemical re-intercalation. The drastic increase in Coulombic inefficiency when the cell is rested at 30 °C indicates that the SEI formation rate dominates at high temperatures. Additionally, the increased lithium self-diffusion has caused the plating to move along the surface, covering a greater portion of the electrode with a thinner layer of lithium. This also exposes more of the lithium surface to electrolyte and reduces the reversibility of the cell. The result suggests that optimal thermal treatment of a cell that experiences lithium plating could involve storage or cycling at low temperatures to mitigate SEI growth.

CHAPTER 4 - VIDEO MICROSCOPY EXPERIMENTS

4.1 Introduction

The consequences of lithium plating range from rapid capacity fade and rise in internal resistance to internal short circuit caused by the growth of dendrites. While many experimental studies have examined the effects of lithium plating on cell lifespan and performance, a complete fundamental understanding of lithium plating behavior is still lacking. Although it is commonly accepted that some portion of plated lithium is reversible, no consistent understanding has been reached concerning the mechanism of re-intercalation of lithium metal deposits. Several researchers have proposed that Li deposits will intercalate “chemically” into graphite, given sufficient time. This view suggests that Li in direct contact with the graphite surface will diffuse into the graphite, potentially leaving a portion of the Li electrically detached. Recently, many models have explored the possibility of electrochemical stripping and intercalation as the cause of reversibility in the Li plating reaction. Lithium stripping is assumed to occur at local anode potentials above 0.0 V, as experienced during the rest phase by the graphite. This process is assumed to be fully reversible, aside from an unknown amount of irreversible losses associated with SEI growth on the plated Li. In this work, a novel technique is developed to observe the relaxation of Li plating directly under an optical microscope in order to verify the occurrence of electrochemical stripping and identify factors that affect the reversibility of the Li plating reaction.

4.2 Objectives

1. To verify the occurrence of electrochemical stripping of lithium plating on graphite during open circuit rest phase following plating.
2. To verify the occurrence of overshooting phase dissolution in graphite during relaxation phase after lithium plating has been induced

4.3 Methodology

4.3.1 Experimental Apparatus

The experimental apparatus used for this set of experiments are the same as discussed in Chapter 3. The M-Braun Glovebox is used for the fabrication of the Li-graphite half cells. The coin cell fabrication process was similar as discussed in Chapter 3. The fabrication of half cells was followed by electrochemical testing for which the Arbin Battery Cycler and the MTI Coin Cell Cycler was used. This set of experiments were conducted under different temperature conditions. The apparatus described in Fig 3.5 was used to perform the low-temperature cases at 0°C. However, the 20°C cases were done in the MTI Coin Cell Cycler in a room that was maintained at 20°C. The electrochemical testing was followed by the quick disassembly of the Li-graphite half-cell in the M-Braun Glove Box. The Leica Si9 microscope was used for capturing the video of the relaxation phase.

4.3.2 Electrochemical Testing

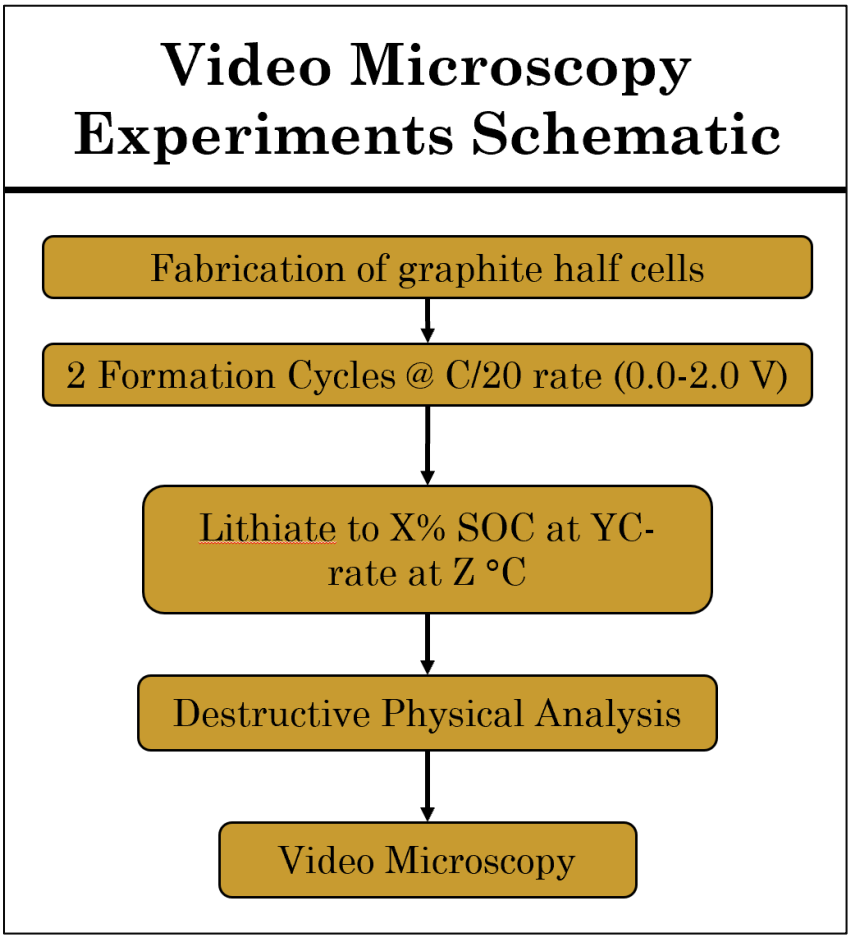

Fig 4.1: Schematic of electrochemical testing protocol followed for the Video Microscopy cases

Fig 4.1 shows the electrochemical testing protocol followed for the video microscopy experiments. The testing starts from the formation cycle of the newly fabricated Li-graphite half cells at a very low C-rate of C/20 between the voltages of 0.0V to 2.0V. Following the formation cycle, isothermal conditions on the cell are established by either using the apparatus shown in Fig 3.5 or in the temperature-controlled room at 20°C. The cell was then lithiated at the specific C-rate for the case which is denoted as Y under an isothermal temperature condition denoted as Z till a specific state of charge denoted by X. Table 4.1 enlists the various cases of video microscopy carried out along with the individual operational parameters in that case.

Table 4.1: List of Video Microscopy experiments performed with their operational parameters

Case	Temperature (Z)	C-rate (Y)	State of Charge (X)
1	0 °C	1C	60%
2	0 °C	C/2	80%
3	0 °C	C/2	80%
4	0 °C	C/2	100%
5	20 °C	1C	100%

4.3.3 Destructive Physical Analysis and Video Microscopy

The electrochemical testing was followed by a quick disassembly of the Li-Graphite half-cell in the Argon filled Glove Box. This was done to ensure that the graphite electrode does not react with the environment thereby leading to the altering of appearance. However, we were interested to observe the changes that the graphite electrode undergoes in the relaxation phase. The graphite electrode was carefully extracted and placed in a case that was filled with the same electrolyte (EC: EMC (3:7 wt%) w/ 1.2 M $LiPF_6$) so that the presence of electrolyte facilitates any electrochemical reactions driven by the local potential difference in the graphite particles. The changes on the graphite electrode were recorded over a stretch of time under the Leica Si9 microscope in the form of a video.

4.4 Results and Discussions

4.4.1 Case 1: 0°C | 1C | 60 SOC

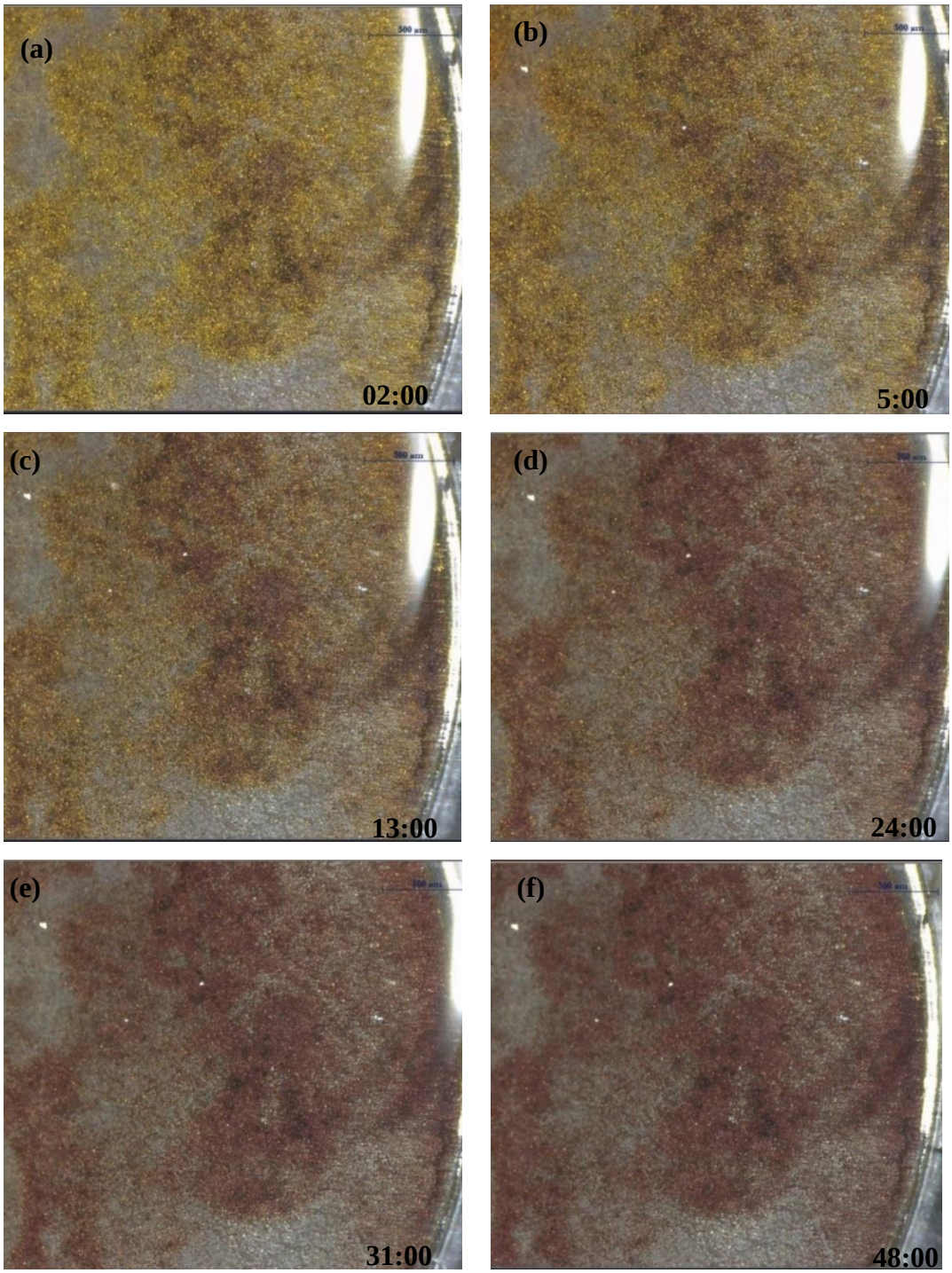

Fig 4.2: Snapshots of video microscopy of relaxation phase for Case 1: 0 °C | 1C | 60% SOC

Snapshots from Video 1 are shown in Fig 4.2 above for Case 1, in which the graphite was lithiated from 0 to 60% SOC at 1C rate at 0 °C. At equilibrium, a graphite electrode at 60% SOC is expected to contain mostly the red stage 2 phase and a small amount of the gold stage 1 phase. However, discharging the cell at a high rate and low temperatures increases the likelihood of overshooting phases, especially at the electrode-separator interface. When the cell was opened, most of the visible electrode surface contained gold, fully lithiated stage 1 graphite. An appreciable amount of silver lithium plating was also found on the surface, along with a small amount of red stage 2 graphite. As the rest phase progressed, almost no changes were observed on the plated lithium metal. The prominent transformation that occurred during rest was the disappearance of the overshooting stage 1 phase and the growth of the stage 2 phase. Since the lithium concentration in each phase is nearly constant, the stage 1 to stage 2 phase transformation results in a rejection of lithium atoms from the interface, which must be compensated by a stage 2L to stage 2 phase transformation in order to conserve the mass of lithium. Therefore, it can be inferred that the electrode from Case 1 initially contained the "undershooting" blue stage 2L at the time the cell was disassembled. Based on our knowledge that fast charging causes high local current density near the electrode-separator interface, it is logical that the low concentration blue phase would be located deep in the electrode near the current collector, where it cannot be observed by the microscope. Case 1 visually confirmed the existence of overshooting stage 1 and implied the existence of some undershooting stage 2L, which both mostly transformed into the dominant stage 2 phase observed prominently at the end of the video when equilibrium was achieved. Another important conclusion from this test is that neither electrochemical stripping nor chemical re-intercalation was observed on the lithium plating over the course of the video.

4.4.2 Case 2: 0 °C | C/2 | 80 SOC

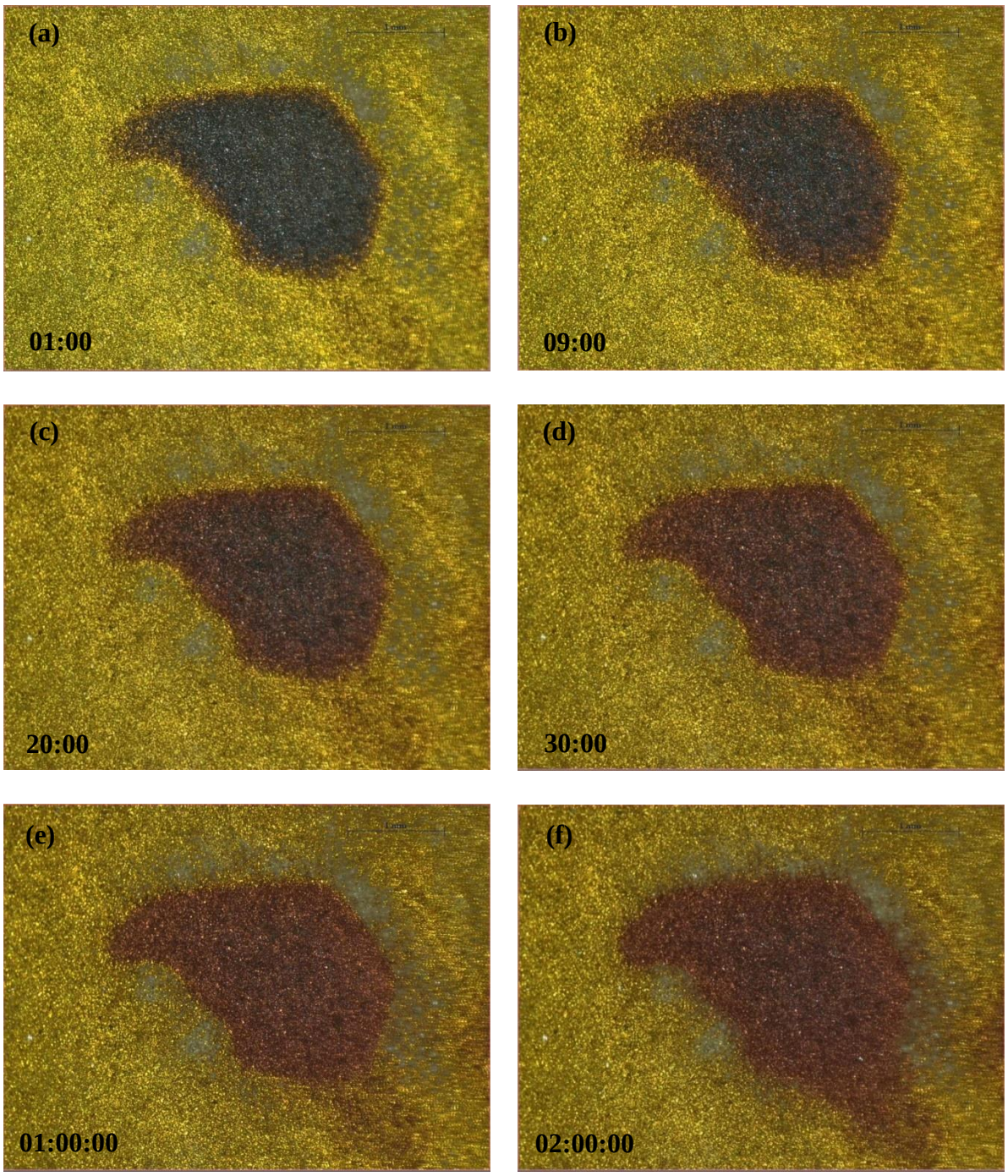

Fig 4.3: Snapshots of video microscopy of relaxation phase for Case 2: 0 °C | C/2 | 80% SOC

Fig 4.3 contains snapshots from the video of Case 2, in which the graphite was lithiated to 80% SOC at 0 °C and C/2 rate. The equilibrium phases for 80% SOC are a mix of gold and red phases,

with the gold stage 1 phase expected to be dominant at the graphite-separator interface. As seen in Fig 4.3(a), a blue and red spot was observed in the center of the electrode in Case 2, which was surrounded by deposits of lithium plating. Similar to Case 1, no macroscopic changes were identifiable on the lithium deposits over the 2 h of recorded video and no electrochemical stripping could be directly observed. In Fig 4.3(b-d), the blue stage 2L gradually turns to red stage 2 over the first 30 min of the video. Whereas in Case 1 the undershooting blue phase was hidden below the electrode surface, Case 2 allows direct observation of the dissolution of blue stage 2L and growth of the red stage 2. In order to supply the additional lithium to drive the 2L → 2 transformation, some gold stage 1 also must transform to stage 2 and the edges of the spot must move outward. Surprisingly, the spot does not expand during this initial 30 min span, suggesting that the phase transformation is driven by plating re-intercalation rather than stage 1 dissolution. Although changes to the film-like lithium deposits were not observed, microscopic lithium deposits could be stripping during this time, bringing the graphite electrode to an overall higher SOC. The spot does not change much before Fig 4.3(e) at the 1 h mark but gradually grows again until the end of the video in Fig 4.3(f) at 2 h. This growth of stage 2 in the latter part of the video could be related to stage 2L dissolution in the depths of the electrode, driven by the local potential difference between the stage 1 and stage 2L phases. Case 2 gives the first indication of a multi-step relaxation process.

4.4.3 Case 3: 0 °C | C/2 | 80 SOC

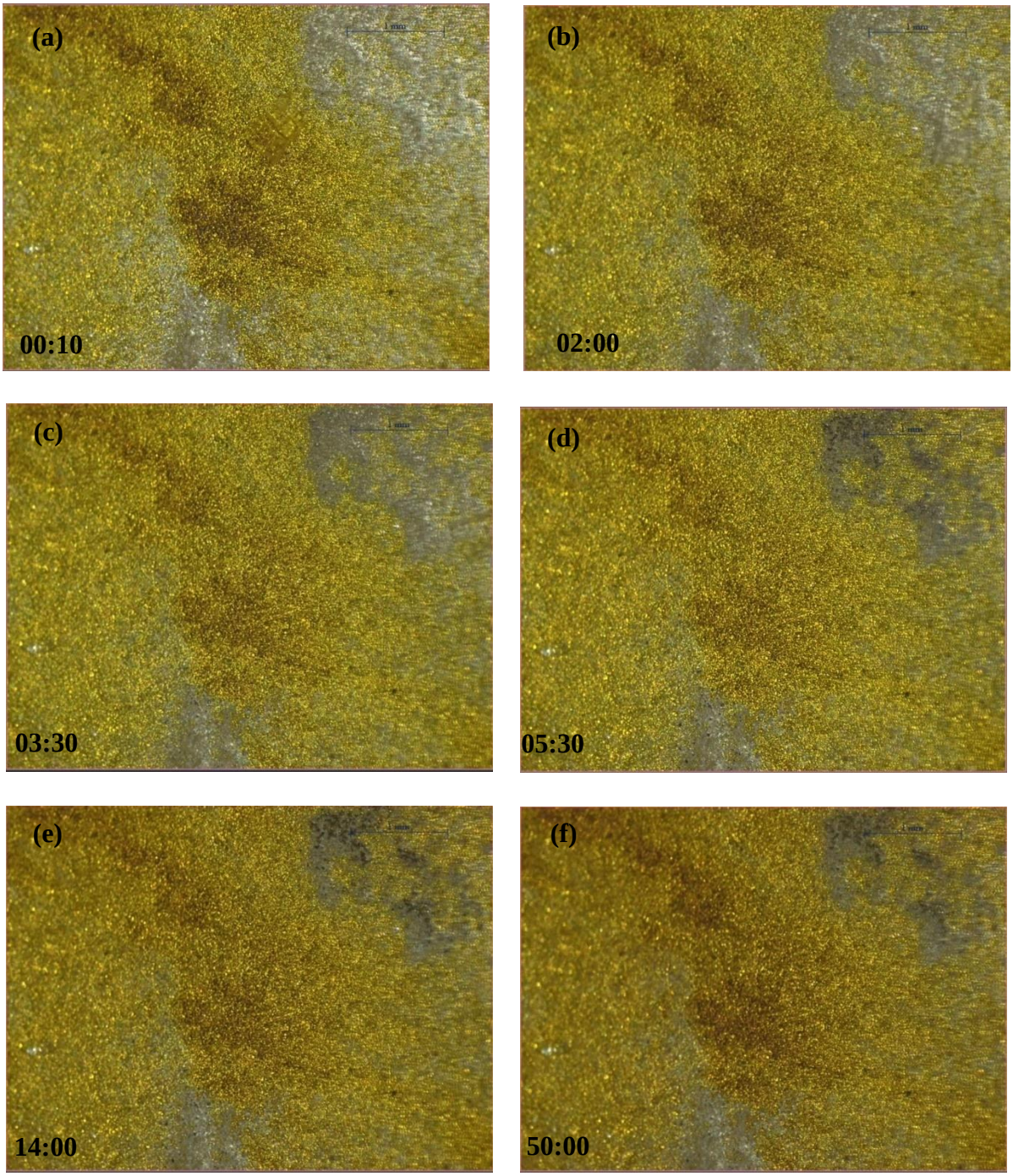

Fig 4.4: Snapshots of video microscopy of relaxation phase for Case 3: 0 °C | C/2 | 80% SOC

Figure 4.4 contains snapshots from Case 3, from the cell which was lithiated to 80% SOC at 0 °C and C/2 rate. At equilibrium, a graphite electrode at 80% SOC should contain a mix of gold and red phases. The surface in view of the microscope is the former electrode-separator interface, which experiences the highest local current density and thus reaches the highest local SOC. Therefore, most of the particles in view throughout Case 3 contain the gold stage 1 phase. Shiny lithium deposits were initially present across much of the electrode surface, as seen in Figure 4.4(a). The deposits become gradually duller and darker over the next 3 minutes and 30 seconds in Figure 4.4(b) and (c). Between 3:30 and 5:30, distinct pit formation occurs on the formerly shiny lithium surface. Concurrently, the amount of red stage 2 graphite in the frame decreases, indicating the re-intercalation of plated lithium. To the best of our knowledge, this is the first direct observation of the phenomenon of electrochemical stripping. After 5:30, no apparent changes occur on the lithium. By the end of the video at 50 minutes, shown in Figure 4.4(e), a small amount of red stage 2 has returned, which indicates the dissolution of the overshooting stage 1 phase.

4.4.4 Case 4: 0°C | C/2 | 100 SOC

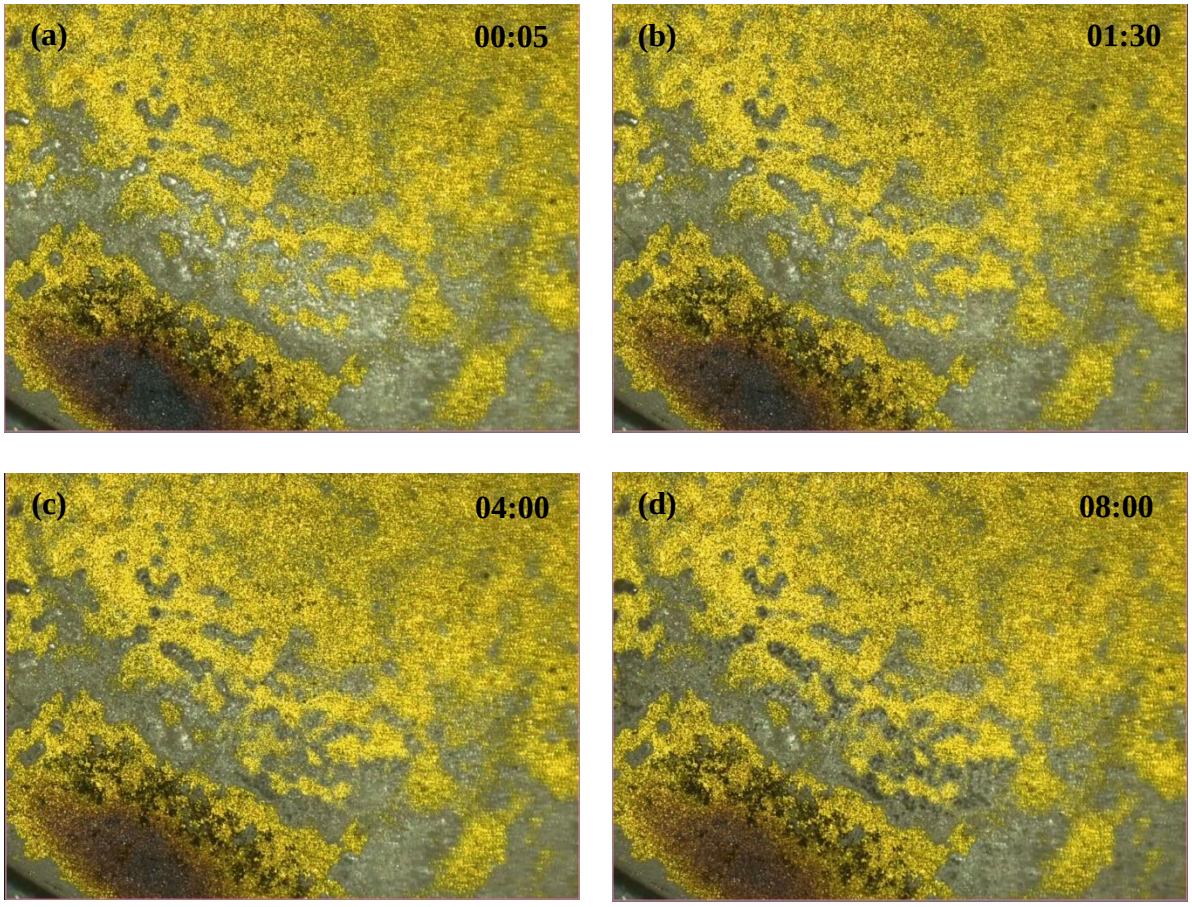

Fig 4.5: Snapshots of video microscopy of relaxation phase for Case 4: 0 °C | C/2 | 100% SOC

Fig 4.5 shows snapshots from the video of Case 4, in which graphite was lithiated to 100% SOC at 0 °C and C/2 rate. In Fig 4.5(a), four phases are initially visible on the graphite surface: stage 2L (blue), stage 2 (red), stage 1 (gold), and lithium plating. The lithium plating has a shiny surface upon disassembly, indicating rounded surfaces. As electrochemical stripping occurs, the lithium surface grows darker and duller in Fig 4.5(b-c). Concurrently, the blue stage 2L phase turns to red stage 2 as more lithium is intercalated into the graphite. By the 8:00 mark, pitting on the lithium metal is distinctly visible, and the red spot has continued to shrink due to re-intercalation.

4.4.5 Case 5: 20 °C | 1C | 100% SOC

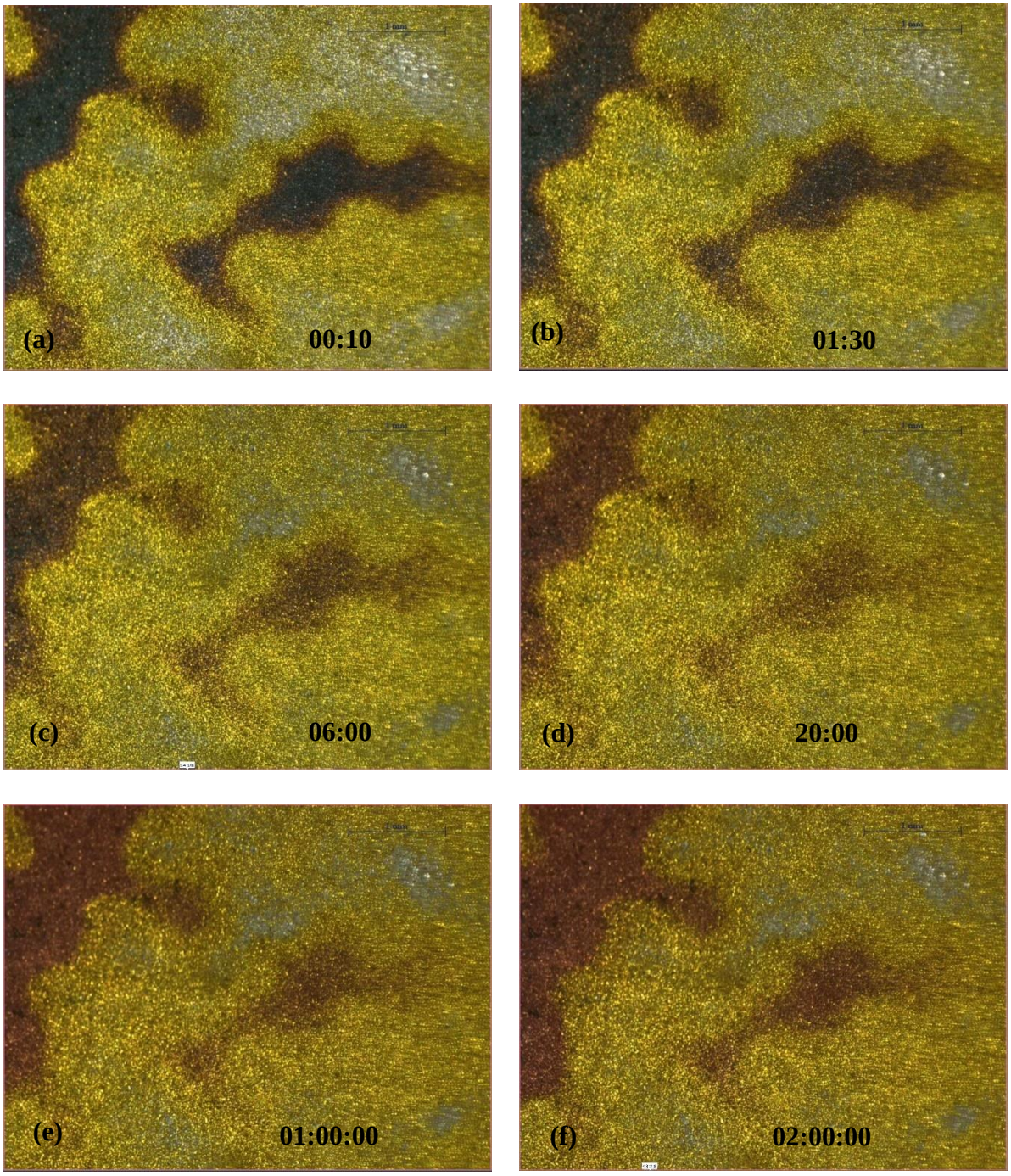

Fig 4.6: Snapshots of video microscopy of relaxation phase for Case 5: 20 °C | 1C | 100% SOC

The results from Case 5 are shown in Fig 4.6 for the case of lithiation to 100% SOC at 1C rate and 20 °C. At 100% SOC, the graphite should contain only the gold stage 1 phase. However, since a portion of the discharge capacity has gone towards lithium plating, the true SOC of the graphite will be less than 100% and the presence of red stage 2 phase is also expected. Upon disassembly of the cell in Fig 4.6(a), the graphite surface contains four phases: stage 2L (blue), stage 2 (red), stage 1 (gold), and lithium plating (silver). The lithium plating is originally shiny but becomes duller and darker by 1:30 in Fig 4.6(b), indicating the occurrence of lithium stripping. The blue phase also starts to turn red during this time. By 6 min in Fig 4.6(c), most of the original lithium deposit has disappeared and the blue phase is nearly completely dissolved. The red spots have also shrunk appreciably by this time. Lithium stripping continues until around 20:00 in Fig 4.6(d), after which no changes to the lithium surface are observed. Gradual growth in the red area occurs in Fig 4.6(e-f) over the ensuing 2 h.

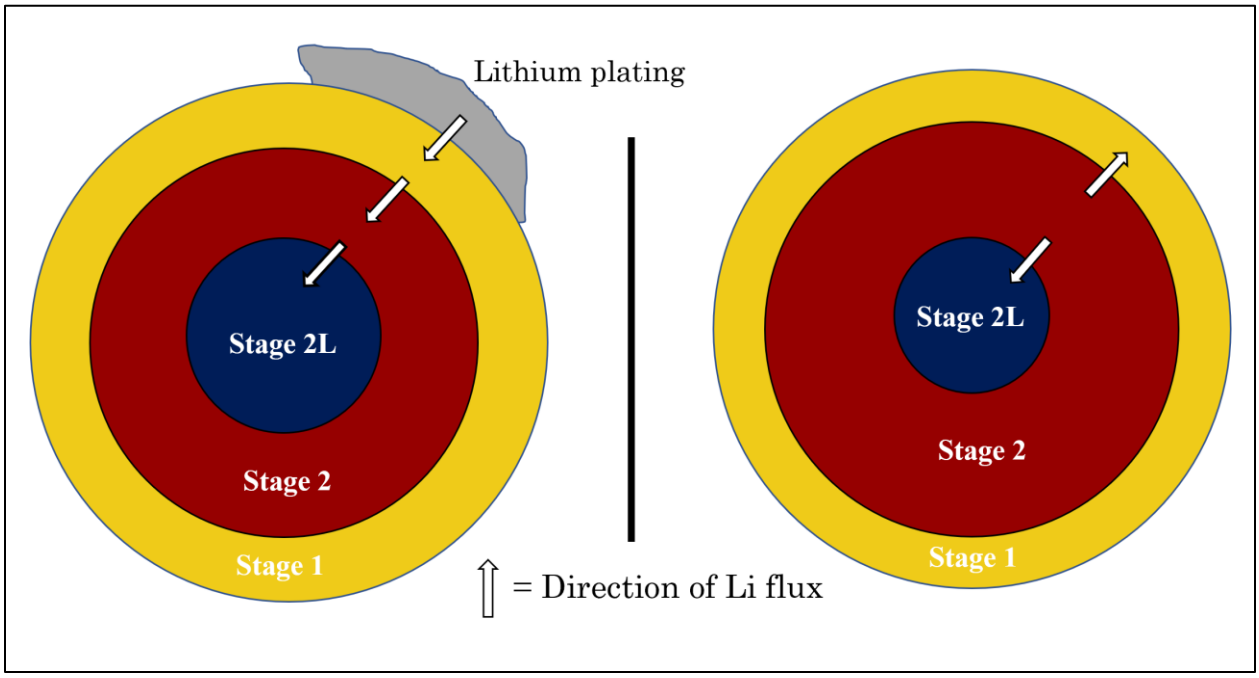

Fig 4.7: Schematic of the color transition during stripping and after stripping

Based on the results of this experiment, the behavior of graphite during the relaxation phase following lithium plating can be summarized as a two-part process, as is schematically depicted in Fig 4.7. First, lithium plating undergoes electrochemical stripping and re-intercalation. During this process, the practical SOC of the graphite increases and the amount of stage 2L phase decreases. Lithium stripping continues until the lithium deposits become electrically isolated, as they can no longer release electrons into the graphite. After the completion of the stripping phase, part 2 of the relaxation process involves the dissolution of stage 1 and stage 2L, accompanied by the growth of the stage 2 phase. Lithium atoms are rejected at the Stage 1 and the Stage 2 interfaces, while they are added at the stage 2 and the stage 2L interfaces. The net result is an expansion of the red stage 2 phase throughout the electrode. Referring back to Fig 3.11(a), the relaxation voltage profiles each contain two plateaus for cells that experienced transport limited plating. While the first plateau is widely ascribed to the lithium stripping process in literature, the second plateau can most likely be ascribed to the process described here as “part 2.”

4.5 Conclusion

In this experiment, the occurrence of electrochemical stripping as well as overshooting phase dissolution was visually confirmed for the first time. In most cases, lithium deposits become less shiny and darker as the relaxation proceeds, indicating a modification of the surface morphology via lithium stripping. Additionally, the formation of pits on the lithium metal surface is evident in many cases. Stripping was not observed for all cases, calling into question the theory that the stripping reaction proceeds spontaneously so long as the graphite potential remains above 0.0 V and electrical connection is maintained between lithium deposits and graphite. Further investigation is needed to determine the physical phenomena of driving or preventing lithium stripping from occurring. A distinct second relaxation process involving the dissolution of overshooting stage 1 and undershooting stage 2L was identified and visually confirmed, validating the work of Bauer et al. [43], [44]. This suggests an explanation for the observation of two plateaus in the relaxation voltage profiles of the transport limited plating in single discharge tests.

No evidence of chemical re-intercalation was identified in these tests. A possible reason is that diffusion of plated lithium into the graphite would rely on adjacent particles having vacancies to store more lithium. However, lithium plating occurs most readily at locations that experience local overcharge due to the heterogeneous distribution of active material in the electrode. Therefore, we have observed that lithium deposits tend to be in contact with stage 1 graphite at the time of cell disassembly. We believe that observation of chemical re-intercalation may require a longer time scale and may only be possible if part 2 of the relaxation process brings particles with stage 2 graphite in contact with the plated lithium deposits. Capturing this process on video will be a subject of future work.

CHAPTER 5 - SUMMARY AND FUTURE WORK

5.1 Summary

While it is widely acknowledged that the lithium plating reaction is detrimental to cell lifespan and is partly reversible, a deep fundamental understanding of the physical processes affecting the behavior of plated lithium is lacking. In this work, the factors affecting the reversibility of the lithium plating reaction were investigated. Reversibility was quantified through Coulombic inefficiency, with the assumption that a negligible portion of the capacity would be used for SEI formation on graphite. The duration and temperature of the rest phase following lithium plating were studied as probable factors influencing the reversibility, with temperature proving itself as the most important factor. Due to the accelerated rate of SEI formation at 30 ℃, the CI nearly doubled as compared to the 0 ℃ case. The minimum efficiency of the lithium plating reaction was found to be 76.6% at 30 ℃, as compared with the minimum efficiency of 86.3% at 0 ℃. This result suggests that cells that have experienced lithium plating should not be exposed to elevated temperatures.

Furthermore, two different strategies were employed to induce lithium plating and their differences were critically examined. To study plating caused by fast charging conditions, defined in this work as transport limited plating, graphite electrodes were initially lithiated to 60% SOC at C/20 rate before discharge pulses of ΔSOC=10, 20, 30, or 40% were applied at 0 ℃ and C/2 rate. To study plating caused by overcharge conditions, defined as kinetically limited plating, electrodes were lithiated to 100% SOC at C/20 rate before discharge pulses of ΔSOC=10, 20, 30, or 40% were applied at 0 ℃ and C/10 rate. Based on previously presented models in the literature, we predicted that the overcharged cells would exhibit a higher degree of reversibility as well as a more homogeneous distribution of plated lithium. The hypothesis was confirmed by the higher CI values and the observation of dense, highly connected films of lithium plating in transport limited cases. The overcharge plating cases exhibited exceptionally low CI for small amounts of overcharge, with a CI of 0.17% at ΔSOC=10%. This kinetically limited condition yielded the highest reversibility for the lithium plating reaction at 98.3% efficiency.

In order to elucidate the complex interplay of relaxation processes, a method was developed to allow for direct observation of the plated graphite electrode during relaxation. Cells were rapidly disassembled, and electrodes were viewed under an optical microscope for several hours. This experiment provided the first direct evidence of electrochemical stripping through the concurrent observation of pit formation on the lithium metal surface and transformation of the blue stage 2L graphite to the red stage 2 phase which contains a higher lithium concentration. A direct observation was also made of the dissolution of overshooting phases in graphite, as described in the work of Bauer *et al.* [43], [44]. This process consists of the dissolution of stage 1 and stage 2L, along with the growth of stage 2 graphite. Based on our observations, a two-part model is proposed for the rest phase processes of graphite under lithium plating conditions.

5.2 Future Work

In the video microscopy experiments, no evidence of the chemical re-intercalation process was obtained. We believe that this process is reliant on direct contact between lithium metal deposits and graphite particles that are not in the fully lithiated state. However, plating tends to occur in locations that experience high local current density and thus reach a high local SOC before the rest of the electrode. In order for chemical re-intercalation to be observed, a longer time scale of observation may be required. If part 2 of the relaxation process brings lithium metal in contact with stage 2 graphite, such as in Fig 4.1, chemical re-intercalation may proceed. Observation of this possible part 3 of the relaxation phase was not possible in this work because the video length was limited by electrolyte evaporation. Future experiments will attempt to suppress the rate of electrolyte evaporation by covering the sample with a quartz lens. This may allow a full realization of the processes at play during relaxation.

REFERENCES

[1] I. Buchmann, *Batteries in a Portable World*, no. July. 2002.

[2] H. Budde-Meiwes *et al.*, "A review of current automotive battery technology and future prospects," *Proc. Inst. Mech. Eng. Part D J. Automob. Eng.*, vol. 227, no. 5, pp. 761–776, 2013.

[3] M. . Thackeray, A. de Kock, and W. I. . David, "SYNTHESIS AND STRUCTURAL CHARACTERIZATION OF DEFECT SPINELS IN THE LITHIUM-MANGANESE-OXIDE SYSTEM," *Археология*, vol. 1, no. August, pp. 117–125, 1993.

[4] N. Martiny and A. Jossen, "Challenges of battery systems in tropical environment," no. June, 2014.

[5] S. Hossain, Y. Saleh, and R. Loutfy, "Carbon-carbon composite as anodes for lithium-ion battery systems," *J. Power Sources*, vol. 96, no. 1, pp. 5–13, 2001.

[6] E. Endo, T. Kihira, S. Yamada, H. Imoto, and K. Sekai, "Surface treatment of carbon electrodes by electron beam irradiation," *J. Power Sources*, vol. 93, no. 1–2, pp. 215–223, 2001.

[7] H. Buqa, C. Grogger, M. V. Santis Alvarez, J. O. Besenhard, and M. Winter, "Surface modification of graphite anodes by combination of high temperature gas treatment and silylation in nonaqueous solution," *J. Power Sources*, vol. 97–98, pp. 126–128, 2001.

[8] C. Natarajan, H. Fujimoto, A. Mabuchi, K. Tokumitsu, and T. Kasuh, "Effect of mechanical milling of graphite powder on lithium intercalation properties," *J. Power Sources*, vol. 92, no. 1–2, pp. 187–192, 2001.

[9] J. W. Fergus, "Fergus-2010-Recent developments1.pdf," vol. 195, pp. 939–954, 2010.

[10] Z. Bin, "'Solid oxide fuel cell (SOFC) technical challenges and solutions from nano-aspects,'" *Int. J. energy Res.*, vol. 31, no. August 2007, pp. 135–147, 2009.

[11] H. Lemmens, "UC San Diego Works to Build Batteries of the Future," 2019. [Online]. Available: https://www.thermofisher.com/blog/microscopy/uc-san-diego-works-to-build-batteries-of-the-future/. [Accessed: 31-Oct-2019].

[12] P. Mohtat *et al.*, "Aging phenomena for Lithium-Ion batteries," *J. Power Sources*, vol. 147, no. December, pp. 98–103, 2017.

[13] Z. Li, J. Huang, B. Yann Liaw, V. Metzler, and J. Zhang, "A review of lithium deposition

in lithium-ion and lithium metal secondary batteries," *J. Power Sources*, 2014.

[14] J. Steiger, G. Richter, M. Wenk, D. Kramer, and R. Mönig, "Comparison of the growth of lithium filaments and dendrites under different conditions," *Electrochem. commun.*, vol. 50, pp. 11–14, 2015.

[15] T. Hirai, I. Yoshimatsu, and J. I. Yamaki, "Effect of Additives on Lithium Cycling Efficiency," *J. Electrochem. Soc.*, vol. 141, no. 9, pp. 2300–2305, 1994.

[16] K. H. Chen *et al.*, "Dead lithium: Mass transport effects on voltage, capacity, and failure of lithium metal anodes," *J. Mater. Chem. A*, vol. 5, no. 23, pp. 11671–11681, 2017.

[17] G. P. Beauregard and A. Z. Phoenix, "Report of investigation: Hybrids plus plug in hybrid electric vehicle," *Natl. Rural Electr. Coop. Assoc. Inc. US Dep. Energy, Idaho Natl. Lab. by etec, Online im Internet URL http//www. evworld. com/library/prius_fire_forensics. pdf [Stand 11.04. 2012]*, 2008.

[18] National Transportation Safety Board, "Auxiliary Power Unit Battery Fire, Japan Airlines Boeing 787-8, JA829J," p. NTSB/AIR-14/01, PB2014-108867, 2014.

[19] P. Stanwick, "Samsung'S Galaxy Note 7: How a Product Can Go Up in Smoke," vol. 5, no. 11, pp. 2016–2019, 2017.

[20] Q. Wang, P. Ping, X. Zhao, G. Chu, J. Sun, and C. Chen, "Thermal runaway caused fire and explosion of lithium ion battery," *J. Power Sources*, vol. 208, pp. 210–224, 2012.

[21] X. Feng, M. Ouyang, X. Liu, L. Lu, Y. Xia, and X. He, "Thermal runaway mechanism of lithium ion battery for electric vehicles: A review," *Energy Storage Mater.*, vol. 10, no. May 2017, pp. 246–267, 2018.

[22] R. Spotnitz and J. Franklin, "Abuse behavior of high-power, lithium-ion cells," *J. Power Sources*, vol. 113, no. 1, pp. 81–100, 2003.

[23] M. Jäckle and A. Groß, "Microscopic properties of lithium, sodium, and magnesium battery anode materials related to possible dendrite growth," *J. Chem. Phys.*, vol. 141, no. 17, 2014.

[24] C. T. Love, O. A. Baturina, and K. E. Swider-Lyons, "Observation of Lithium Dendrites at Ambient Temperature and Below," *ECS Electrochem. Lett.* , vol. 4, no. 2, pp. A24–A27, Jan. 2015.

[25] S. J. Harris, A. Timmons, D. R. Baker, and C. Monroe, "Direct in situ measurements of Li transport in Li-ion battery negative electrodes," *Chem. Phys. Lett.*, vol. 485, no. 4–6, pp.

265–274, 2010.

[26] J. Steiger, D. Kramer, and R. Mönig, “Mechanisms of dendritic growth investigated by in situ light microscopy during electrodeposition and dissolution of lithium,” *J. Power Sources*, vol. 261, pp. 112–119, 2014.

[27] M. Fleischhammer, T. Waldmann, G. Bisle, B.-I. Hogg, and M. Wohlfahrt-Mehrens, “Interaction of cyclic ageing at high-rate and low temperatures and safety in lithium-ion batteries,” *J. Power Sources*, vol. 274, pp. 432–439, Jan. 2015.

[28] T. Waldmann and M. Wohlfahrt-Mehrens, “Effects of rest time after Li plating on safety behavior—ARC tests with commercial high-energy 18650 Li-ion cells,” *Electrochim. Acta*, vol. 230, pp. 454–460, 2017.

[29] N. Legrand, B. Knosp, P. Desprez, F. Lapicque, and S. Raël, “Physical characterization of the charging process of a Li-ion battery and prediction of Li plating by electrochemical modelling,” *J. Power Sources*, vol. 245, pp. 208–216, 2014.

[30] C. H. Doh, B. C. Han, B. S. Jin, and H. B. Gu, “Structures and formation energies of LixC6 (x=1-3) and its homologues for lithium rechargeable batteries,” *Bull. Korean Chem. Soc.*, vol. 32, no. 6, pp. 2045–2050, 2011.

[31] P. Arora, M. Doyle, and R. E. White, “Mathematical modeling of the lithium deposition overcharge reaction in lithium-ion batteries using carbon-based negative electrodes,” *J. Electrochem. Soc.*, vol. 146, no. 10, pp. 3543–3553, 1999.

[32] K. Tokumitsu, H. Fujimoto, A. Mabuchi, and T. Kasuh, “High capacity carbon anode for Li-ion battery a theoretical explanation,” *Carbon N. Y.*, vol. 37, no. 10, pp. 1599–1605, 1999.

[33] J. Shim and K. A. Striebel, “Effect of electrode density on cycle performance and irreversible capacity loss for natural graphite anode in lithium-ion batteries,” *J. Power Sources*, vol. 119–121, pp. 934–937, 2003.

[34] H. Buqa, D. Goers, M. Holzapfel, M. E. Spahr, and P. Novák, “High rate capability of graphite negative electrodes for lithium-ion batteries,” *J. Electrochem. Soc.*, vol. 152, no. 2, pp. 474–481, 2005.

[35] T. Ohzuku, Y. Iwakoshi, and K. Sawai, “Formation of Lithium-Graphite Intercalation Compounds in Nonaqueous Electrolytes and Their Application as a Negative Electrode for a Lithium Ion (Shuttlecock) Cell,” *J. Electrochem. Soc.*, vol. 140, no. 9, pp. 2490–

2498, 1993.

[36] F. Cao, I. V. Barsukov, H. J. Bang, P. Zaleski, and J. Prakash, “Evaluation of graphite materials as anodes for lithium-ion batteries,” *J. Electrochem. Soc.*, vol. 147, no. 10, pp. 3579–3583, 2000.

[37] D. Guerard and A. Herold, “Intercalation of lithium into graphite and other carbons,” *Carbon N. Y.*, vol. 13, no. 4, pp. 337–345, 1975.

[38] R. Fong, U. von Sacken, and J. R. Dahn, “Studies of Lithium Intercalation into Carbons Using Nonaqueous Electrochemical Cells,” vol. 137, no. 7, pp. 3–7, 2009.

[39] J. . Dahn, R. Fong, and M. J. Spoon, “Suppression of staging in lithium-intercalated carbon by disorder in the host,” *Zhongguo Youse Jinshu Xuebao/Chinese J. Nonferrous Met.*, vol. 21, no. 5, pp. 1045–1051, 2011.

[40] M. Heß and P. Novák, “Shrinking annuli mechanism and stage-dependent rate capability of thin-layer graphite electrodes for lithium-ion batteries,” *Electrochim. Acta*, vol. 106, pp. 149–158, 2013.

[41] A. Shellikeri *et al.*, “Investigation of pre-lithiation in graphite and hard-carbon anodes using different lithium source structures,” *J. Electrochem. Soc.*, vol. 164, no. 14, pp. A3914–A3924, 2017.

[42] J. Wandt, P. Jakes, J. Granwehr, R. A. Eichel, and H. A. Gasteiger, “Quantitative and time-resolved detection of lithium plating on graphite anodes in lithium ion batteries,” *Mater. Today*, vol. 21, no. 3, pp. 231–240, 2018.

[43] M. Bauer, M. Wachtler, H. Stöwe, J. V. Persson, and M. A. Danzer, “Understanding the dilation and dilation relaxation behavior of graphite-based lithium-ion cells,” *J. Power Sources*, vol. 317, pp. 93–102, 2016.

[44] M. Bauer *et al.*, “Multi-phase formation induced by kinetic limitations in graphite-based lithium-ion cells: Analyzing the effects on dilation and voltage response,” *J. Energy Storage*, vol. 10, pp. 1–10, Apr. 2017.

[45] E. Peled, “The Electrochemical Behavior of Alkali and Alkaline Earth Metals in Nonaqueous Battery Systems—The Solid Electrolyte Interphase Model,” *J. Electrochem. Soc.*, vol. 127, no. 6, p. 1324, 1980.

[46] M. Yoshio, R. J. Brodd, and A. Kozawa, *Lithium-ion batteries : science and technologies / Masaki Yoshio, Ralph J. Brodd, Akiya Kozawa, editors.* 2009.

[47] J. O. Besenhard, M. Winter, J. Yang, and W. Biberacher, “Filming mechanism of lithium-carbon anodes in organic and inorganic electrolytes,” *J. Power Sources*, vol. 54, no. 2, pp. 228–231, 1995.

[48] M. Inaba *et al.*, “Electrochemical scanning tunneling microscopy observation of highly oriented pyrolytic graphite surface reactions in an ethylene carbonate-based electrolyte solution,” *Langmuir*, vol. 12, no. 6, pp. 1535–1540, 1996.

[49] M. Inaba, Z. Siroma, Y. Kawatate, A. Funabiki, and Z. Ogumi, “Electrochemical scanning tunneling microscopy analysis of the surface reactions on graphite basal plane in ethylene carbonate-based solvents and propylene carbonate,” *J. Power Sources*, vol. 68, no. 2, pp. 221–226, 1997.

[50] M. Nie, D. Chalasani, D. P. Abraham, Y. Chen, A. Bose, and B. L. Lucht, “Lithium ion battery graphite solid electrolyte interphase revealed by microscopy and spectroscopy,” *J. Phys. Chem. C*, vol. 117, no. 3, pp. 1257–1267, 2013.

[51] M. Herstedt, D. P. Abraham, J. B. Kerr, and K. Edström, “X-ray photoelectron spectroscopy of negative electrodes from high-power lithium-ion cells showing various levels of power fade,” *Electrochim. Acta*, vol. 49, no. 28, pp. 5097–5110, 2004.

[52] A. M. Andersson, D. P. Abraham, R. Haasch, S. MacLaren, J. Liu, and K. Amine, “Surface characterization of electrodes from high power lithium-ion batteries,” *J. Electrochem. Soc.*, vol. 149, no. 10, pp. 1358–1369, 2002.

[53] Q. Liu *et al.*, “Understanding undesirable anode lithium plating issues in lithium-ion batteries,” *RSC Adv.*, vol. 6, no. 91, pp. 88683–88700, 2016.

[54] J. Jaguemont, L. Boulon, and Y. Dubé, “A comprehensive review of lithium-ion batteries used in hybrid and electric vehicles at cold temperatures,” *Appl. Energy*, vol. 164, pp. 99–114, 2016.

[55] L. Gireaud, S. Grugeon, S. Laruelle, B. Yrieix, and J. M. Tarascon, “Lithium metal stripping/plating mechanisms studies: A metallurgical approach,” *Electrochem. commun.*, vol. 8, no. 10, pp. 1639–1649, 2006.

[56] M. Petzl, M. Kasper, and M. A. Danzer, “Lithium plating in a commercial lithium-ion battery - A low-temperature aging study,” *J. Power Sources*, vol. 275, pp. 799–807, 2015.

[57] M. Petzl and M. A. Danzer, “Nondestructive detection, characterization, and quantification of lithium plating in commercial lithium-ion batteries,” *J. Power Sources*,

vol. 254, pp. 80–87, 2014.

[58] M. C. Smart, B. V. Ratnakumar, L. Whitcanack, K. Chin, M. Rodriguez, and S. Surampudi, “Performance characteristics of lithium ion cells at low temperatures,” *Proc. Annu. Batter. Conf. Appl. Adv.*, vol. 2002-Janua, pp. 41–46, 2002.

[59] T. Waldmann *et al.*, “Interplay of operational parameters on lithium deposition in lithium-ion cells: Systematic measurements with reconstructed 3-electrode pouch full cells,” *J. Electrochem. Soc.*, vol. 163, no. 7, pp. A1232–A1238, 2016.

[60] T. Waldmann, B. I. Hogg, and M. Wohlfahrt-Mehrens, “Li plating as unwanted side reaction in commercial Li-ion cells – A review,” *J. Power Sources*, vol. 384, no. November 2017, pp. 107–124, 2018.

[61] S. P. Rangarajan, Y. Barsukov, and P. P. Mukherjee, “ In operando signature and quantification of lithium plating ,” *J. Mater. Chem. A*, vol. 7, no. 36, pp. 20683–20695, 2019.

[62] T. Waldmann, M. Wilka, M. Kasper, M. Fleischhammer, and M. Wohlfahrt-Mehrens, “Temperature dependent ageing mechanisms in Lithium-ion batteries - A Post-Mortem study,” *J. Power Sources*, vol. 262, pp. 129–135, 2014.

[63] V. Zinth *et al.*, “Lithium plating in lithium-ion batteries at sub-ambient temperatures investigated by in situ neutron diffraction,” *J. Power Sources*, vol. 271, pp. 152–159, 2014.

[64] J. Fan and S. Tan, “Studies on charging lithium-ion cells at low temperatures,” *J. Electrochem. Soc.*, vol. 153, no. 6, 2006.

[65] J. Li, E. Murphy, J. Winnick, and P. A. Kohl, “The effects of pulse charging on cycling characteristics of commercial lithium-ion batteries,” *J. Power Sources*, vol. 102, no. 1–2, pp. 302–309, 2001.

[66] B. K. Purushothaman and U. Landau, “Rapid charging of lithium-ion batteries using pulsed currents,” *J. Electrochem. Soc.*, vol. 153, no. 3, 2006.

[67] Y. Ji and C. Y. Wang, “Heating strategies for Li-ion batteries operated from subzero temperatures,” *Electrochim. Acta*, vol. 107, pp. 664–674, 2013.

[68] M. C. Smart and B. V. Ratnakumar, “Effects of electrolyte composition on lithium plating in lithium-ion cells,” *J. Electrochem. Soc.*, vol. 158, no. 4, pp. 379–389, 2011.

[69] B. V. Ratnakumar and M. C. Smart, “Lithium plating behavior in lithium-ion cells,” *ECS*

Trans., vol. 25, no. 36, pp. 241–252, 2010.

[70] H. S. Song *et al.*, "Experimental study on the effects of pre-heating a battery in a low-temperature environment," *2012 IEEE Veh. Power Propuls. Conf. VPPC 2012*, pp. 1198–1201, 2012.

[71] M. R. Giuliano, A. K. Prasad, and S. G. Advani, "Experimental study of an air-cooled thermal management system for high capacity lithium-titanate batteries," *J. Power Sources*, vol. 216, pp. 345–352, 2012.

[72] K. Persson, Y. Hinuma, Y. S. Meng, A. Van Der Ven, and G. Ceder, "Thermodynamic and kinetic properties of the Li-graphite system from first-principles calculations," *Phys. Rev. B - Condens. Matter Mater. Phys.*, vol. 82, no. 12, pp. 1–9, 2010.

[73] F. Hao, A. Verma, and P. P. Mukherjee, "Mesoscale Complexations in Lithium Electrodeposition," *ACS Appl. Mater. Interfaces*, vol. 10, no. 31, pp. 26320–26327, 2018.

[74] J. Arai, Y. Okada, T. Sugiyama, M. Izuka, K. Gotoh, and K. Takeda, "In situ solid state ^{7}Li NMR observations of lithium metal deposition during overcharge in Lithium Ion Batteries," *J. Electrochem. Soc.*, vol. 162, no. 6, pp. A952–A958, 2015.

[75] D. Aurbach, I. Weissman, A. Schechter, and H. Cohen, "X-ray photoelectron spectroscopy studies of lithium surfaces prepared in several important electrolyte solutions. A comparison with previous studies by fourier transform infrared spectroscopy," *Langmuir*, vol. 12, no. 16, pp. 3991–4007, 1996.

[76] T. Waldmann *et al.*, "Review - Post-mortem analysis of aged lithium-ion batteries: Disassembly methodology and physico-chemical analysis techniques," *J. Electrochem. Soc.*, vol. 163, no. 10, pp. A2149–A2164, 2016.

[77] A. Hightower, C. C. Ahn, B. Fultz, and P. Rez, "Electron energy-loss spectrometry on lithiated graphite," *Appl. Phys. Lett.*, vol. 77, no. 2, pp. 238–240, 2000.

[78] C. Uhlmann, J. Illig, M. Ender, R. Schuster, and E. Ivers-Tiffée, "In situ detection of lithium metal plating on graphite in experimental cells," *J. Power Sources*, vol. 279, pp. 428–438, 2015.

[79] J. Steiger, D. Kramer, and R. Mönig, "Microscopic observations of the formation, growth and shrinkage of lithium moss during electrodeposition and dissolution," *Electrochim. Acta*, vol. 136, pp. 529–536, 2014.

[80] O. Crowther and A. C. West, "Effect of electrolyte composition on lithium dendrite

growth," *J. Electrochem. Soc.*, vol. 155, no. 11, pp. 806–811, 2008.

[81] H. Honbo, K. Takei, Y. Ishii, and T. Nishida, "Electrochemical properties and Li deposition morphologies of surface modified graphite after grinding," *J. Power Sources*, vol. 189, no. 1, pp. 337–343, 2009.

[82] M. Zier *et al.*, "Lithium dendrite and solid electrolyte interphase investigation using OsO4," *J. Power Sources*, vol. 266, pp. 198–207, 2014.

[83] N. Ghanbari, T. Waldmann, M. Kasper, P. Axmann, and M. Wohlfahrt-Mehrens, "Detection of Li Deposition by Glow Discharge Optical Emission Spectroscopy in Post-Mortem Analysis," *ECS Electrochem. Lett.* , vol. 4, no. 9, pp. A100–A102, Jan. 2015.

[84] S. S. Zhang, K. Xu, and T. R. Jow, "Study of the charging process of a LiCoO2-based Li-ion battery," *J. Power Sources*, vol. 160, no. 2 SPEC. ISS., pp. 1349–1354, 2006.

[85] M. S. Wu, P. C. J. Chiang, and J. C. Lin, "Electrochemical investigations on advanced lithium-ion batteries by three-electrode measurements," *J. Electrochem. Soc.*, vol. 152, no. 1, pp. 47–52, 2005.

[86] L. Yang *et al.*, "Lithium deposition on graphite anode during long-term cycles and the effect on capacity loss," *RSC Adv.*, vol. 4, no. 50, pp. 26335–26341, 2014.

[87] G. Nagasubramanian and D. H. Doughty, "18650 Li-ion cells with reference electrode and in situ characterization of electrodes," *J. Power Sources*, vol. 150, no. 1–2, pp. 182–186, 2005.

[88] J. R. Belt, D. M. Bernardi, and V. Utgikar, "Development and Use of a lithium-metal reference electrode in aging studies of lithium-ion batteries," *J. Electrochem. Soc.*, vol. 161, no. 6, pp. 1116–1126, 2014.

[89] A. N. Jansen, D. W. Dees, D. P. Abraham, K. Amine, and G. L. Henriksen, "Low-temperature study of lithium-ion cells using a LiySn micro-reference electrode," *J. Power Sources*, vol. 174, no. 2, pp. 373–379, 2007.

[90] M. D. Levi *et al.*, "Solid-State Electrochemical Kinetics of Li-Ion Intercalation into Li," *Society*, vol. 146, no. 4, pp. 1279–1289, 1999.

[91] F. La Mantia, C. D. Wessells, H. D. Deshazer, and Y. Cui, "Reliable reference electrodes for lithium-ion batteries," *Electrochem. commun.*, vol. 31, pp. 141–144, 2013.

[92] Y. Hoshi, Y. Narita, K. Honda, T. Ohtaki, I. Shitanda, and M. Itagaki, "Optimization of reference electrode position in a three-electrode cell for impedance measurements in

lithium-ion rechargeable battery by finite element method," *J. Power Sources*, vol. 288, pp. 168–175, 2015.

[93] B. Bitzer and A. Gruhle, "A new method for detecting lithium plating by measuring the cell thickness," *J. Power Sources*, vol. 262, pp. 297–302, 2014.

[94] C. Birkenmaier, B. Bitzer, M. Harzheim, A. Hintennach, and T. Schleid, "Lithium plating on graphite negative electrodes: Innovative qualitative and quantitative investigation methods," *J. Electrochem. Soc.*, vol. 162, no. 14, pp. A2646–A2650, 2015.

[95] F. B. Spingler, W. Wittmann, J. Sturm, B. Rieger, and A. Jossen, "Optimum fast charging of lithium-ion pouch cells based on local volume expansion criteria," *J. Power Sources*, vol. 393, no. May, pp. 152–160, 2018.

[96] J. C. Burns, D. A. Stevens, and J. R. Dahn, "In-situ detection of lithium plating using high precision coulometry," *J. Electrochem. Soc.*, vol. 162, no. 6, pp. A959–A964, 2015.

[97] I. D. Campbell, M. Marzook, M. Marinescu, and G. J. Offer, "How Observable Is Lithium Plating? Differential Voltage Analysis to Identify and Quantify Lithium Plating Following Fast Charging of Cold Lithium-Ion Batteries," *J. Electrochem. Soc.* , vol. 166, no. 4, pp. A725–A739, Jan. 2019.

[98] X. G. Yang, S. Ge, T. Liu, Y. Leng, and C. Y. Wang, "A look into the voltage plateau signal for detection and quantification of lithium plating in lithium-ion cells," *J. Power Sources*, vol. 395, no. May, pp. 251–261, 2018.

[99] S. Schindler, M. Bauer, M. Petzl, and M. A. Danzer, "Voltage relaxation and impedance spectroscopy as in-operando methods for the detection of lithium plating on graphitic anodes in commercial lithium-ion cells," *J. Power Sources*, vol. 304, pp. 170–180, Feb. 2016.

[100] D. Anseán *et al.*, "Operando lithium plating quantification and early detection of a commercial LiFePO4 cell cycled under dynamic driving schedule," *J. Power Sources*, vol. 356, pp. 36–46, 2017.

[101] D. Ren *et al.*, "Investigation of Lithium Plating-Stripping Process in Li-Ion Batteries at Low Temperature Using an Electrochemical Model," *J. Electrochem. Soc.* , vol. 165, no. 10, pp. A2167–A2178, Jan. 2018.

PUBLICATIONS

IN PREPARATION

1. **T. Adhikary**, C. Fear, and P. P. Mukherjee, "In Operando video microscopy of lithium plating", December 2019

2. C. Fear, **T. Adhikary**, R. Carter, C. T. Love, and P. P. Mukherjee, "Examination of Reversibility of Lithium Plating", December 2019

3. C. Fear, **T. Adhikary**, R. Carter, C. T. Love, and P. P. Mukherjee, "Detection and Characterization of the Onset of Lithium Plating during Fast Charging of Lithium-ion Batteries", December 2019